Arabian Journal of Chemistry (2020) 13, 1466–1489

King Saud University

Arabian Journal of Chemistry

www.ksu.edu.sa
www.sciencedirect.com

ORIGINAL ARTICLE

Selenotriapine – An isostere of the most studied thiosemicarbazone with pronounced pro-apoptotic activity, low toxicity and ability to challenge phenotype reprogramming of 3-D mammary adenocarcinoma tumors

Nenad R. Filipović [a], Snežana K. Bjelogrlić [b], Sveva Pelliccia [c], Vesna B. Jovanović [d], Milan Kojić [e], Milan Senćanski [f], Giuseppe La Regina [g], Romano Silvestri [g], Christian D. Muller [h,*], Tamara R. Todorović [d,*]

[a] *Faculty of Agriculture, University of Belgrade, Nemanjina 6, Belgrade, Serbia*
[b] *National Cancer Research Center of Serbia, Pasterova 14, Belgrade, Serbia*
[c] *Dipartimento di Farmacia, Università di Napoli "Federico II", via D. Montesano 49, 80131 Naples, Italy*
[d] *Faculty of Chemistry, University of Belgrade, Studentski trg 12-16, Belgrade, Serbia*
[e] *Laboratory for Molecular Microbiology, Institute of Molecular Genetics and Genetic Engineering, University of Belgrade, Belgrade, Serbia*
[f] *Center for Multidisciplinary Research, Institute of Nuclear Sciences "Vinča", University of Belgrade, Belgrade, Serbia*
[g] *Dipartimento di Chimica e Tecnologie del Farmaco, Laboratory affiliated to Istituto Pasteur-Fondazione Cenci Bolognetti, Sapienza UniversitaÃ di Roma, Piazzale Aldo Moro 5, I-00185 Roma, Italy*
[h] *Institut Pluridisciplinaire Hubert Curien, UMR 7178 CNRS Université de Strasbourg, 67401 Illkirch, France*

Received 15 September 2017; accepted 23 November 2017
Available online 28 November 2017

KEYWORDS

Selenosemicarbazone;
3-D culture;
Apoptosis;
Mitochondrial superoxide production;
Oct-4

Abstract Triapine, the most studied α-*N*-heterocyclic thiosemicarbazone, revealed potent activity against advanced leukemia, but was ineffective against a variety of solid tumors. Moreover, methemoglobinemia, which is a side effect of triapine administration, may limits all clinical application. To enhance anticancer activity and reduce side effects, we applied an isosteric replacement of sulfur to selenium atom was performed by synthesis and characterization of selenium triapine analog, 3-aminopyridine-2-carboxaldehyde selenosemicarbazone (selenotriapine). Compared to triapine,

* Corresponding authors.
E-mail addresses: cdmuller@unistra.fr (C.D. Muller), tamarat@chem.bg.ac.rs (T.R. Todorović).
Peer review under responsibility of King Saud University.

Production and hosting by Elsevier

https://doi.org/10.1016/j.arabjc.2017.11.017

selenotriapine revealed superior pro-apoptotic activity with activation of intrinsic apoptotic pathway in both human monocytic leukemia (THP-1) and mammary adenocarcinoma (MCF-7) cell lines. For MCF-7 2-D cultures, selenotriapine induced notable increase in mitochondrial superoxide radical generation and dissipation of mitochondrial transmembrane potential. A significant delay in growth of MCF-7 spheroids (3-D culture) was accompanied by phenotypic stem cell reprogramming (Oct-4 expression). Additionally, selenotriapine demonstrated a very low toxicity profile as compared to triapine, confirmed over alleviated extent of methemoglobin formation and higher IC_{50} value in brine shrimp cytotoxicity assay.

1. Introduction

Anticancer properties of α-*N*-heterocyclic thiosemicarbazones, known tridentate *N,N,S* chelators, were studied starting from the late 1960s (French et al., 1974). After it was shown that 5-hydroxy-2- carboxaldehyde thiosemicarbazone (5-HP), the first thiosemicarbazone which entered phase I clinical trials, possesses minimal antileukemic activity (DeConti et al., 1972), in order to find more potent drug candidates multiple novel 5-HP derivatives have been developed. From a group of pyridine-substituted thiosemicarbazones, 3-aminopyridine-2-carboxaldehyde thiosemicarbazone (Triapine, 3-AP) emerged as the most potent anticancer compound against mouse lymphocytic leukemia (L1210) cells (Cory et al., 1994, 1995; Finch et al., 2000; Liu et al., 1992, 1996). In vitro activity of 3-AP has been observed in leukemia, non-small-cell lung cancer, renal cancer, and melanoma cell lines (Schelman et al., 2009). 3-AP has been the most studied thiosemicarbazone-based anticancer agent with more than 30 clinical phase I and phase II trials. First mechanistic studies showed that 3-AP exerts its antineoplastic activity by inhibiting DNA synthesis and repair, and it was recognized as a potent small molecule ribonucleotide reductase (RR) inhibitor (Cory et al., 1994). Human RR is tetramer complex composed of two non-identical homodimers, hRRM1 and hRRM2, responsible for the reduction of ribonucleotides to deoxyribonucleotides. The large subunit hRRM1 harbors the catalytic site, allosteric effector-binding sites, and redox active disulfides that participate in the reduction of substrates, whereas the small subunit hRRM2 contains an oxygen-linked di-ferric center and one tyrosyl radical per monomer that are essential for enzymatic activity. A protein p53R2 is 80% hRRM2 homolog which plays a crucial role in supplying deoxyribonucleotides for DNA repair (Shao et al., 2004; Aggarwal et al., 2007). There are two pathways in human cells to supply deoxyribonucleotides for DNA synthesis: one through the activity of hRRM2 involved in normal maintains of deoxyribonucleotides for DNA replication during the S-phase in a cell cycle dependent manner, and the other one through p53R2, supplying deoxyribonucleotides for DNA repair during G0/G1 phase that is p53 dependent (Shao et al., 2004). RR plays a fundamental role in the critical early events involved in tumor promotion and its activity is tightly linked to the neoplastic expression state and is currently one of the main targets for DNA inhibition by anticancer agents (Moorthy et al., 2013). Sartoreli et al. revealed that 3-AP inhibits incorporation of [^{3}H] thymidne into DNA while incorporation of cytidine into DNA via RR was markedly inhibited, thus a pronounced decrease in the formation of [^{14}C] deoxyribonucleotides from radioactive cytidine occurs in the acid-soluble fraction of 3-AP-treated L1210 cells (Cory et al., 1994). Later it was shown that 3-AP is equally potent inhibitor of hRRM2 and p53R2, which was not the case for other chelating agents (Shao et al., 2004). The following mechanisms of RR inhibition by 3-AP, based on inactivation of its active site, have been proposed: (1) direct destruction of active site by Fe(III) chelation; (2) indirect destruction of active site by Fe(II)-3-AP complex obtained by the reaction of 3-AP with iron from cellular pool(s); (3) indirect destruction of active site by reactive oxygen species (ROS) generated during reaction of dioxygen with Fe(II)-3-AP obtained from reduction of Fe(III)-(3-AP) by endogenous reductants; (4) direct reduction of tyrosyl radical by Fe(II)-(3-AP) complex without ROS formation; (5) endoplasmic reticulum stress induction; (6) mitochondrial ROS production (Aye et al., 2012; Myers, 2016; Myers et al., 2011; Trondl et al., 2014). It is still not completely elucidated if there is a prevailing source of iron that is particularly susceptible for chelating reaction with 3-AP. Recent studies have revealed that there is no formation of Fe(III)-3-AP in blood and 3-AP is not able to sequester iron from iron-binding proteins such as holo-transferrin or hemoglobin (Pelivan et al., 2016), while the transiently increased ferritin levels indicate that the interaction of 3-AP with iron occurs in the liver which is known as the site of ferritin production (Wadler et al., 2004).

Despite the fact that 3-AP showed promising activity against advanced leukemia in clinical phase I trials, several clinical phase II studies revealed that 3-AP is ineffective against a variety of solid tumors, indicating increased expression of multidrug-resistance proteins as the main cause (Heffeter et al., 2012). Side effects associated with 3-AP administration are hypoxia and methemoglobinemia, resulting from the oxidation of oxyhemoglobin (oxyHb) to methemoglobin (metHb), which limit its clinical application considering it can compromise cardiopulmonary function of patients. The ability of 3-AP to form a redox active iron complex is an important factor in the formation of metHb (Quach et al., 2012). In order to deal with 3-AP side effects, to understand its mechanism of action in more detail and to improve its efficacy, various strategies have been employed such as management of methemoglobinemia by supplemental oxygen and intravenous administration of therapeutic antidotes (Kunos et al., 2012), synthesis of various 3-AP derivatives (Cory et al., 1994; Kowol et al., 2016; Quach et al., 2012; Stefani et al., 2013), and synthesis of d-metal complexes with 3-AP as a ligand (Basha et al., 2016; Enyedy et al., 2010, 2011; Ishiguro et al., 2014; Myers et al., 2013; Pelivan et al., 2016).

Selenium analogues of thiosemicarbazones have been investigated to a much smaller extent due to controversial about selenium impact on health. First, this element was marked as toxic, but in 1980s was found to be essential in humans (Combs Jr., 2015). Despite the fact that selenium chemistry is more similar to sulfur than to oxygen, the difference between two heavier chalcogens is particularly pronounced in terms of redox behavior, which has been referred as the selenium paradox. As comparative studies showed, the nature of chalcogen atom has a great impact on biological activity of isosteric selenosemicarbazones and thiosemicarbazones (Al-Eisawi et al., 2016; Calcatierra et al., 2015; Klayman et al., 1983; Kowol et al., 2012; Mautner et al., 1956; Molter et al., 2011; Pizzo et al., 2012; Revenko et al., 2011). Both classes of compounds equally inhibit herpes simplex virus type-1 ribonucleoside diphosphate reductase (Turk et al., 1986). Thiosemicarbazones were found to be more effective antineoplastic and antimalaric agents than selenosemicarbazones (Klayman et al., 1983), which on the other hand are more selective toward neoplastic cells relative to normal ones (Al-Eisawi et al., 2016). Selenium compounds also showed better antiproliferative and antimicrobial activity, plus superior cruzipain inhibition when compared to the sulfur analogues (Mautner et al., 1956; Pizzo et al., 2012; Revenko et al., 2011). Our recent study showed that selenium compounds are less toxic in comparison to their sulfur analogues (Filipovic et al., 2017). Selenosemicarbazones also coordinate iron in a tridentate fashion and consequently they are capable to inhibit RR (Agrawal et al., 1974; West et al., 1985). ROS production, oxidative stress as well as mitochondrial membrane disruption and lysosomal membrane permeabilization are found to be involved in the mechanism of cytotoxic activity of selenosemicarbazones (Filipovic et al., 2016). Our recent study demonstrated that this class of compounds possess strong differentiation-inducing ability (Todorovic et al., 2017).

In this work, isosteric replacement of sulfur to selenium atom was performed by synthesis and characterization of selenium analog of 3-AP, 3-aminopyridine-2-carboxaldehyde selenosemicarbazone (Se-3-AP). Our investigations provide information on how malignant in vitro biological models are affected by the treatment with Se-3-AP. The pro-apoptotic activities of both compounds were tested in parallel on two human cell lines: an acute monocytic leukemia (THP-1) and a mammary adenocarcinoma (MCF-7) cell lines. Activity of 3-AP has been evaluated against leukemia (Cory et al., 1994; Finch et al., 1999, 2000; Karp et al., 2008; Trondl et al., 2014), but published results on THP-1 cells harboring mutated p53 are still missing (Leitch et al., 2016). 3-AP was also investigated for the treatment of breast cancer in two clinical trials (Mortazavi et al., 2013; Schelman et al., 2009), whereas in vitro results of its activity on MCF-7 cells with wild-type p53 was determined by means of colorimetric assay after 6 day incubation (Jordheim et al., 2005). Relying on previous reports that showed 3-AP-mediated inhibition of RR abrogates homologous recombinant repair (HRR) (Lin et al., 2014), we chose cell lines with different p53 status as a good model to compare modes of 3-AP and Se-3-AP activities. A body of evidences revealed that wild-type p53 suppresses HRR activity, whereas in cells that express mutated p53 activity of HRR is stimulated although not statistically significant compared to those with fully functional p53 (Bertrand et al., 2004; Gatz and Wiesmuller, 2006; Liu et al., 2010; Mekeel et al., 1997; Ratner et al., 2016). Additionally, we investigated activity of Se-3-AP on 3-D spheroid model, which according to its architecture well mimics in vivo tumor mass in a function of multiple parameters (Lin and Chang, 2008), particularly due to recognized feature of breast cancer cell lines to re-establish phenotypic equilibrium of the parental tumor (Gupta et al., 2011). Toxicity profile of both compounds regarding metHb formation and *Artemia salina* lethality assay was also analyzed.

2. Experimental

2.1. Reagents and instrumentation

tert-Butyl (2-formylpyridin-3-yl)carbamate and 3-AP were synthesized according reported procedures (Kowol et al., 2009). All other chemicals and solvents (reagent grade) were obtained from commercial suppliers and used without further purification. Elemental analyses (C, H, N) were performed by the standard micromethods using the ELEMENTAR Vario EL III CHNS/O analyzer at Center for Instrumental Analysis, Faculty of Chemistry – University of Belgrade. Elemental analyses are within $\pm 0.4\%$, confirming $>95\%$ purity. IR spectra were recorded on a Thermo Scientific Nicolet 6700 FT-IR spectrophotometer by the Attenuated Total Reflection (ATR) technique in the region 4000–350 cm^{-1}. Abbreviations used for IR spectra: vs very strong; s, strong; m, medium; w, weak. The NMR spectra were performed on a Bruker Avance 500 equipped with broad-band direct probe. Chemical shifts are given on δ scale relative to tetramethylsilane (TMS) as internal standard for ^{1}H and ^{13}C, or indirect referencing to TMS as ^{1}H standard for ^{77}Se. All spectra were measured at 298 K. Abbreviations used for NMR data: s, singlet; m, multiplet; py, pyridine; Cq, py = pyridine quaternary carbon atom. pH values were measured using a CRISON pH-Burette 242S equipped with a CRISON 50 29 micro-combined pH electrode (CRISON INSTRUMENTS, S.A. Spain). For acidity constants determination, UV/vis spectra were recorded on a Thermo Scientific Evolution 60S spectrophotometer (Thermo Fisher Scientific Inc, Waltham, Massachusetts, USA) using a quartz cell with 1.0 cm path length. For DPPH scavenging activity, absorbance at 517 nm was measured using a Thermo Scientific Appliskan. Anticancer related experiments were performed on Guava® easyCyte 12HT Benchtop flow microcapillary cytometer (EMD Millipore, Darmstadt, Germany) using the InCyte® software package (EMD Millipore, Cat. No. 0500-4120). A Submarine Mini-gel Electrophoresis Unit (Hoeffer HE 33) with an EPS 300 power supply was used for DNA cleavage studies. The stained gel was illuminated under a UV trans illuminator Vilber-Lourmat (France) at 312 nm and photographed with a Nikon Coolpix P340 Digital Camera through filter Deep Yellow 15 (Tiffen, USA). For HSA binding experiments UV/vis spectra were recorded on a UV-1800 Shimadzu spectrophotometer (Shimadzu, Japan) equipped with thermostat bath, against the corresponding blank (0.1 M PBS pH 7.4) in the range 250–450 nm. The fluorescence measurements were performed on a FluoroMax-4 Jobin Yvon (Horiba Scientific, Japan) spectrofluorometer equipped with

1.0 cm quartz cell and thermostat bath. The excitation and emission slit widths were set to 6.5 nm.

2.2. Synthesis of 3-aminopyridine-2-carbaldehyde selenosemicarbazone (Se-3-AP)

To a mixture of *tert*-butyl (2-formylpyridin-3-yl)carbamate (1.468 g, 6.61 mmol) and selenosemicarbazide (662 mg, 7.27 mmol) in EtOH/H_2O solvent mixture (22.5 mL, 67% v/v), 3 mL of conc. HCI was added. The resulting solution was refluxed for 3 h, cooled down to a room temperature (RT) and resulting precipitate was filtered of. The crude yellowish Se-3-AP × HCl was transferred into a flask and 40 mL of hot water and 10% aq. $NaHCO_3$ (8 mL) was added. The mixture was stirred at RT for 1 h (at pH 7.0). The crude product was filtered of and washed with water (10 mL), EtOH (3 mL) and Et_2O (10 mL). The obtained solid was dried under high vacuum for a few hours. Yield: 0.28 g (66%). Anal. Calcd. for $C_7H_9N_5Se$ (M_r 242.14): C, 34.72; H, 3.75; N, 28.92. Found: C, 34.52; H, 3.61; N, 28.90%. UV/vis (DMSO), λ_{max}, nm (ε, M^{-1} cm^{-1}): 316 (5947), 393 (21248). IR (ATR, cm^{-1}): 3398 (vs), 3300 (vs), 1626 (vs), 1542 (s), 1451 (s), 1366 (m), 1318 (w), 1266 (s), 1147 (m), 1053 (w), 803 (w), 749 (w). ^{1}H NMR (500 MHz, DMSO d_6): δ 11.57 (s, 1H, N—NH), 8.58 (s, 1H, Se=C—NH_2), 8.45 (s, 1H, Se=C—NH_2), 8.43 (s, 1H, HC=N), 7.84 (s, 1H, H_{py}), 7.19–7.04 (m, 2H, H_{py}), 6.47 (s, 2H, NH_2). ^{13}C NMR (126 MHz, DMSO d_6): δ 172.33 (C=Se), 150.61 (C=N), 144.17 (C_q, C_{py}CH), 137.28(C_{py}), 132.45 (C_q, $C_{py}NH_2$), 124.69 (C_{py}), 122.37 (C_{py}). ^{77}Se NMR (95 MHz, DMSO d_6): δ 203.50.

2.3. Cyclic voltammetry

The cell (10 mL) consisted of three-electrode system: glassy carbon electrode (inner diameter of 3 mm; CHI 104), an Ag/AgCl (saturated KCl) reference electrode and Pt counter electrode. The potential was swept over the range from 2.0 to +1.2 V (*vs.* Ag/AgCl) at scan rate of 100 mV s^{-1}. Measurements were performed at RT with deaeration by passing a stream of nitrogen through the solution for 5 min prior to the measurement and then maintaining a blanket atmosphere of nitrogen over the solution during the measurements. The potentials were measured in 0.10 M tetrabutylammonium hexafluorophosphate/DMSO, and are quoted relative to Ag/AgCl reference electrode.

2.4. Determination of acidity constants

Acidity constants of Se-3-AP were determined by spectrophotometric titration at t = 25 ± 1 °C. Working solution (c = 0.031 mM) was prepared by dissolving accurately weighted dried Se-3-AP in 5 mL of DMSO; 10 mM phosphate buffer (pH 1.77, I = 0.1 M NaCl) was added up to 100 mL. First, pH value was adjusted to 1.65 with conc. HCl, than small volume increments of 1 M KOH were added stepwise, until pH 11.88 was reached (total volume change at the end of the titration was lower than 2%). During titration, after each pH value equilibration, pH values were continuously measured and UV/vis spectra were recorded. The spectra were recorded at following pH values: 1.73, 1.98, 2.25, 2.50, 2.82, 3.19, 3.70, 3.89, 4.09, 4.33, 4.55, 4.88, 5.21, 5.50, 5.82, 6.49, 9.19, 9.58, 9.79, 9.98, 10.20, 10.50, 10.95, 11.41, 11.88, against the phosphate buffer as a blank. The pH electrode was calibrated by standard CRISON buffer solutions (pH 4.01, 7.00, and 9.21). Acidity constants were calculated according to transformed forms of classical spectrophotometric equations (Albert and Serjeant, 1984).

2.5. Free radical scavenging antioxidant assay

The proton donating ability of Se-3-AP and 3-AP was assayed using a protocol for the determination of radical scavenging activity (Prior et al., 2005). Compounds were dissolved in pure DMSO and were diluted into ten different concentrations. Commercially available free radical DPPH was dissolved in methanol at a concentration of 6.58×10^{-5} M. Into a 96-well microplate, 140 μL of DPPH solution was loaded and 10 mL DMSO solution of the tested compounds was added, or pure DMSO (10 μL) as the control. The microplate was incubated for 30 min at 298 K in the dark and the absorbance was measured at 517 nm. All the measurements were carried out in triplicate. The scavenging activity of the compounds was calculated using Eq. (1):

$$\text{Scavenging activity}(\%) = [(A_{control} - A_{sample})/A_{control}] \times 100 \quad (1)$$

where A_{sample} and $A_{control}$ refer to the absorbance at 517 nm of DPPH in the sample and control solutions, respectively.

IC_{50} values were calculated from the plotted graph of scavenging activity against the concentrations of the samples. IC_{50} is defined as the total antioxidant concentration necessary to decrease the amount of the initial DPPH radical by 50%. IC_{50} was calculated for all compounds based on the percentage of DPPH radicals scavenged. Vitamin C was used as the reference compound (positive control) with concentrations 50–500 μg × mL^{-1}.

2.6. Cell cultures

Human mammary adenocarcinoma (MCF-7, ATCC® HTB-22) cell line was maintained in Dulbecco's Modified Eagle's high glucose Medium (DMEM, Dominique Dutscher, 67172 Brumath cedex, France, Cat No L0102-500), while human acute monocytic leukemia cell line (THP-1, ATCC® TIB-202) was maintained in Roswell Park Memorial Institute 1640 medium (RPMI-1640, Life Technologies, Paisley, UK, Cat. No. 11875-093), supplemented with 10% (v/v) heat inactivated fetal bovine serum (FBS, Life Technologies, Paisley, UK, Cat No 10270-106) and 1% (v/v) penicillin-streptomycin (10,000 U/mL and 10,000 μg/mL Life Technologies, Paisley, UK, Cat No 15140-122). Cells were kept at 37 °C in humidified atmosphere containing 5% (v/v) CO_2 during their exponential growing phase and in the course of incubation with investigated compounds. Investigated compound was initially dissolved in DMSO to the stock concentration of 20 mM. Further dilutions to the experimental concentrations applied on the cells have been done with RPMI-1640 or DMEM media immediately before each experiment, thus the final concentration of DMSO on cells treated with the highest applied concentration was 0.5% (v/v).

2.7. Evaluation of pro-apoptotic activity

Cells were seeded in 96 flat bottom well plates (Corning® Costar®, Cat. No. CLS3596) in a volume 0.1 mL, at a density of 10,000 per well. MCF-7 cells were left overnight to settle, while treatment of THP-1 cells started 2 h after seeding. Investigated compounds were added in a range of six concentrations. As controls, non-treated cells, cells treated with 0.5% DMSO, and cells treated with Celastrol (Enzo Life Sciences, Cat. No. ALX-350-332-M025) at 50 μM concentration were used. After 24 h of incubation, from wells with treated MCF-7 cells supernatant medium with non-adherent cells were removed into another 96 well plate. Fresh PBS was added to remaining adherent cells afterwards the plate was centrifuged at 450*g* for 10 min. Supernatant was discarded and 200 μL of trypsin-EDTA (BioWest, Nuaille, France, Cat No L0930-100) was added to each well. Cells were detached in about 15 min of incubation at 37 °C. Trypsin-EDTA was removed after additional spinning cycle, afterwards previously removed supernatants with non-adherent cells were added to trypsinized cells and stained with Annexin V-FITC (Immuno Tools, Friesoythe, Germany, Cat No 31490013) and PI (Miltenyl Biotec Inc, Auburn, USA, Cat No 130-093-233) in volumes of 3 μL. In the case of THP-1 cells, Annexin V-FITC and PI were added to the wells with cells right after the incubation time was over. Described trypsinization protocol was applied each time MCF-7 cells were prepared for flow cytometry analyses, unless is stated otherwise. Plates were analyzed and classified according to AnnexinV-FITC (green fluorescence) and PI (red fluorescence) labeling on viable (double negative), pre-apoptotic cells (Annexin V-FITC single-stained cells), necrotic cells (PI single-stained cells), and cells in advanced phases of apoptosis (double-stained cells).

2.8. ED_{50} determination

Percentages of Annexin V single-stained and double-stained cells were summarized for each concentration of investigated compound. The computed percentages were potted against corresponding concentrations on a concentration-response graph. ED_{50} concentration was calculated as the one that corresponds to a half-way of the sigmoidal concentration-dependent curve using asymmetric five-parameter logistic equation (GraphPad Prism 6 software).

2.9. Cell cycle analysis

Distribution of cells within phases of mitotic division has been evaluated on remaining cells after Annexin V-FITC/PI analysis. Right after pro-apoptotic read out was finished, cells were fixed in EtOH overnight at 4 °C, and afterwards stained with FxCycle PI/RNAse Staining solution (Molecular Probes, Cat. No. F10797), and analyzed on a microcapillary flow cytometer.

2.10. Inhibition of caspase activity

Cells were treated with investigated compound at ED_{50} concentration for 6 h with or without pan-caspase inhibitor Z-VAD-fmk (Promega, Madison, USA, Cat. No. G7232). As controls, non-treated cells, cells treated with Z-VAD-fmk only, and cells treated with ED_{50} concentration only were used. After incubation period was ended, treated cells were carried out for Annexin V/PI staining as described above, and analyzed on a cytometer. The percent of apoptosis inhibited by Z-VAD-fmk co-treatment was determined by Eq. (2):

$$\text{apoptosis inhibition}(\%) = [1 - (\%\ \text{of apoptosis in A}/\%\ \text{of apoptosis in B})] \times 100 \quad (2)$$

where A is the sample treated with Z-VAD-fmk and investigated compound applied at ED_{50} concentration, while B is the corresponding sample treated with investigated compound at ED_{50} concentration only.

2.11. Evaluation of caspase-8 and -9 activities

Cells were treated with investigated compound at ED_{50} concentration for 6 h afterwards activity of caspase-8 and -9 were assayed by means of Guava Caspase 9 SR and Caspase 8 FAM kit (EMD Millipore, Cat. No. 4500-0640), following manufacturer's instructions. Cells were analyzed on flow microcapillary cytometer. In acquired data cells were discriminated according to expression of activated caspase-8, caspase-9, or both.

2.12. Assessment of changes in mitochondrial transmembrane potential

Cells were treated over 6 h with investigated compound in concentration of 50 μM. After incubation was terminated, cells were trypsinized and stained with FlowCellect MitoDamage Kit (Merck Millipore Corporation, Darmstadt, Germany, Cat. No. FCCH100106) according to manufacturer's recommendations. Analysis has been performed on flow microcapillary cytometer. Cells were classified according to labeling with Annexin V-FITC, MitoSense Red, and 7-AAD.

2.13. Determination of mitochondrial superoxide radical generation

Cells were treated over 6 h with investigated compounds in concentration of 50 μM, afterwards were stained with MitoSox Red (Molecular Probes, Cat. No. M36008) according to manufacturer's recommendations. Analysis has been performed on a flow microcapillary cytometer.

2.14. Growth inhibition of 3-D tumor models

3-D MCF-7 tumor models were made in 96 well plates (Corning, Sigma-Aldrich, St. Louis, Mo, USA, Cat No 4515). Tumors were left to grow for additional four days, afterwards investigated compound was added in concentrations of 1, 10, and 100 μM. Evaluation has been maintained during 8-day incubation period, with media exchanged on day 4. Changes in the tumors sizes have been assessed on Celigo® imaging cytometer estimating the area of spheroids' cross section (Cyntellect, Brooks Life Science Systems, Poway, CA, USA) using Celigo software. Growth rates of non-treated and treated spheroids were computed for each day during 8-day incubation by dividing the area on the day n with the area on the day 0.

2.15. Detection of gene expression in live cells

After 8-day incubation, non-treated and treated spheroids were transferred to flat bottom 96 well plate (Corning® Costar®, Cat. No. CLS3596), and segregated by trypsin in several consecutive courses (BioWest, Nuaille, France, Cat No L0930-100) with gently repeated pipetting. After spheroids were completely dissociated into single cell suspensions, samples were treated according to recommendations of manufacturer with SmartFlare RNA probes (Millipore, Merck, Darmstadt, Germany) or not (non-stained control): scrambled control (negative control, Cat No SF-102), uptake control (Cat No SF-114) and Oct-4 (Cat No SF-460). Incubation with SmartFlare probes lasted for 16 h at 37 °C in humidified atmosphere containing 5% (v/v) CO_2, afterwards all samples were trypsinized and analyzed on a flow microcapillary cytometer.

2.16. DNA damage experiments

The ability of 3-AP and Se-3-AP to inhibit Cu(I)-driven plasmid DNA damage was assayed using a literature protocol (Battin et al., 2011). Breafly, $CuSO_4$ (6 μM), the indicated concentrations of 3-AP/Se-3-AP, EtOH (10 mM), deionized H_2O, 3-(*N*-morpholino)propanesulfonic acid (10 mM), NaCl (130 mM), and ascorbic acid (1.25 equiv; 7.5 mM) were mixed at pH 7 and allowed to stand for 5 min at room temperature. Plasmid (pUC19, 0.1 pmol in 10 mM TrisHCl pH 8) was added to each reaction mixture and the solutions were again allowed to stand for additional 5 min. The hydroxyl radical formation was initiated by the addition of H_2O_2 (50 mM). After 30 min, EDTA (50 mM) was added to quench the reactions.

2.17. Determination of metHb

Blood sample from healthy human donor was collected in Vacutainer collection tubes (BD, Plymouth, UK) and used immediately. RBC were isolated by centrifugation (480*g* for 5 min at 4 °C) and then were washed in physiological solution. To prepare RBC lysates, RBC were lysed with miliQ water, the debris was removed by centrifugation (13000*g* for 30 min at 4 °C), and the supernatant was used ([oxyHb] = 4.4 mM). Working solutions of oxyHb (1.5 and 0.1 mM) were prepared by dilution using 0.1 mM PBS (pH 7.4). Stock solutions of Se-3-AP (5 mM) and 3-AP (5mM) were prepared by dissolving an appropriate amount of substance in DMSO and further diluted in 0.1 mM PBS (pH 7.4). The total content of DMSO in tested samples was less than 0.5% (vol.%). Concentrations of oxyHb and metHb were determined at 577 and 630 nm.

2.18. UV/vis and fluorescence spectroscopy

The working solutions of Se-3-AP different concentrations, as indicated in the text, for UV/vis and fluorescence spectroscopy were prepared by diluting the stock solution of Se-3-AP (5 mM) with 0.1 M PBS (pH 7.4) or DMSO. A stock solution of Se-3-AP (5 mM) was prepared daily by dissolving an appropriate amount of substance in DMSO.

2.19. HSA binding experiments

Fatty acid free HSA (< 0.007% fatty acids, M_w 66 478 Da) was purchased from Sigma. A stock solution of HSA (0.25 mM) was prepared by dissolving an accurately weighed mass of HSA in freshly prepared 0.1 M PBS (pH 7.4), and kept in a freezer in 100 μL portions. A stock solution of Se-3-AP (5 mM) was prepared daily by dissolving an appropriate amount of substance in DMSO. Millipore water was used for all aqueous solutions.

Binding of Se-3-AP to HSA was studied by fluorescence quenching titration method using the intrinsic fluorescence of HSA as probe. For fluorescence studies, solutions of HSA and Se-3-AP were prepared daily by diluting the stock solutions of HSA and Se-3-AP with 100 mM PBS pH 7.4 or DMSO to the final concentrations of HSA (0.125 μM) and Se-3-AP (80 μM), respectively. Before recording the fluorescence spectrum, diluted HSA solution was ultrafiltered using filters with 0.45 μm pore size. Small aliquots of 80 μM Se-3-AP solutions were added to 2.5 mL of 0.125 μM HSA solution. The Se-3-AP was added in 1.5, 3, 4, 5, 6, 7, 8, 9, 10, 11, 12, 13, 14 and 15 M equivalents, so after the last equivalent, the total DMSO did not exceed 2.4% in volume. After each aliquot addition, the system was stirred and left to equilibrate for 5 min before fluorescence emission spectra were recorded in the range 300–450 nm with an excitation wavelength of 280 nm and 0.1 s integration time. Spectra represent the average of three accumulations and the background buffer signal was subtracted from each spectrum. Fluorescence quenching data were corrected for the inner-filter effect and further processed (for details see Supplementary data).

2.20. Docking to HSA

Se-3-AP was optimized at B97D DFT level of theory (Grimme, 2006), using LanL2DZ basis set for Se (Dunning and Hay, 1977; Hay and Wadt, 1985), and 6-311G + (d,p) basis set for C, N and H atoms (Krishnan et al., 1980; McLean and Chandler, 1980). Geometrical optimization was carried in Gaussian 09, revision D.01 (Frisch et al., 2016). Ligand was afterwards prepared for docking in ADT Tools 1.5.6 (Morris et al., 2009; Sanner, 1999). Three HSA crystal structures (PDB IDs: 1BJ5 (Curry et al., 1998), 2BXD (Ghuman et al., 2005), and 4L9Q (Wang et al., 2013) were obtained from the Protein Data Bank (http://www.rcsb.org/pdb). The active sites were identified according to positions of crystallized ligands in the PDB structures. Ligands were removed, as well as water and ions and structures were prepared for docking using Autodock Tools 1.5.6 (Morris et al., 2009; Sanner, 1999). Docking was carried in AutodockVina 1.1.2 (Trott and Olson, 2010). The grid box size was set to 24 × 24 × 24 Å and exhaustiveness to 250. All calculations were carried on PARADOX computer cluster (Scientific Computing Laboratory of the Institute of Physics, Belgrade, Serbia).

2.21. Artemia salina toxicity assay

A teaspoon of lyophilized eggs of the brine shrimp *Artemia salina* was added to a vessel filled with 1 L of the artificial sea

water containing several drops of yeast suspension (3 mg of dry yeast in 5 mL of distilled water). The vessel was partially exposed to illumination and with assisted water aeration kept for 48 h at 28 °C. After hatching, nauplii were collected by pipette at the illuminated side of the vessel. Tested compounds were dissolved in DMSO (1 mg/100 μL) immediately before the experiment. Five working concentrations have been made with artificial seawater and added to vials which contained 10–20 hatched nauplii, thus the final concentrations of investigated compounds were in the range 0.01–5 mg/mL. $K_2Cr_2O_7$ in the same concentration range served as positive control. Vials with nauplii, sea water and DMSO in concentrations that corresponded to those in experimental samples (0.1–5%) served as a negative control. All vials were left at 28 °C, under illumination, and water aeration for 24 h, afterwards live and dead nauplii were counted. The LC_{50} concentration was determined as the one that induced death of 50% nauplii in treated population. Each experimental sample has been performed in duplicates.

2.22. Statistical analysis

Analyzed data were expressed in three replicates each obtained from different experiments. The statistical significance of differences was assessed using unpaired *t* test with Welch's correction, or one-way ANOVA followed by unpaired *t* test with Welch's correction depending on number of groups to compare, which is specifically notified in figure captions.

3. Results

3.1. Chemistry

The three step synthesis of Se-3-AP, with an overall yield of 66%, started from 3-amino-2-bromopyridine (Scheme 1). The protection of amino group with di*tert*-butyl dicarbonate (Boc_2O) in dry THF was achieved using sodium bis-(trimethylsilyl)amide as a base (Kowol et al., 2009). The *tert*-Boc protected 3-amino-2-bromopyridine was than treated with *n*-butyllithium (*n*-BuLi) in dry THF to obtain lithiated species, which was further converted to carboxaldehyde by treatment with *N*-formylpiperidine (Kowol et al., 2009). Condensation reaction between ethanolic solutions of *tert*-Boc protected 3-amino-2-formylpyridine carboxaldehyde and selenosemicarbazide in the presence of conc. HCl afforded Se-3-AP × HCl. Hydrochloride salt was converted into Se-3-AP by treatment with sodium bicarbonate. 3-AP was synthesized as previously reported (Kowol et al., 2009).

Characterization of Se-3-AP was done by means of UV/vis, fluorescence and 1-D and 2-D NMR spectroscopy (Figs. S1–S8, Supplementary data). In ^{1}H NMR spectrum of Se-3-AP in dimethylsulfoxide (DMSO)-d_6 just one set of signals could be observed, with the N-NH signal at 11.57 ppm. This indicates, as previously observed for 3-AP and related 2-formylpyridine thiosemicarbazones (Kowol et al., 2016; Pessoa et al., 2001), that Se-3-AP exists in *E*-isomeric form. In the UV/vis spectrum of Se-3-AP absorptions at 316 nm (weak) and at 393 nm (strong) were found, while there is a maximum at 457 nm in emission spectrum irradiated at λ_{ex} = 360 nm in DMSO. The redox behavior of Se-3-AP and 3-AP has been investigated by cyclic voltammetry in the potential range from +1.2 to –2.0 V relative to Ag/AgCl reference electrode. In the cyclic voltammogram of both Se-3-AP and 3-AP (Fig. S9, Supplementary data) there is one well defined oxidation peak (Se-3-AP: +0.661 V; 3-AP: +0.628 V) and one reduction peak (Se-3-AP: –0.857 V; 3-AP: –0.951 V).

The proton-dissociation processes of Se-3-AP were followed by UV/vis spectrophotometric titration. Since Se-3-AP is poorly soluble in water, 5% (v/v) DMSO/water solvent mixture was found to be suitable media for aqueous solution equilibrium study. UV/vis spectra of Se-3-AP in the pH ranges 1.73–6.49 and 6.49–11.88 are shown in Fig. 1. Two proton-dissociation processes could be determined (Scheme 2) with two well separated ($\Delta pK_a > 3$) pK_avalues ($pK_{a1} = 4.23 \pm 0.01$ at 404 nm and $pK_{a2} = 9.75 \pm 0.04$ at 296 nm), as indicated by clearly visible isosbestic points in the two pH regions. Characteristic spectral changes of Se-3-AP can be observed in the 250–450 nm wavelength range. Se-3-AP displays two intense absorption bands due to $n \rightarrow \pi^*$ transitions of the pyridine ring and the selenosemicarbazide moiety (Filipovic et al., 2016). During the first deprotonation step ($[H_2A]^+ \rightarrow [HA]$), a blue shift and a decrease in intensity of the absorption maximum in the visible region and a redshift and a decrease in absorption maximum in the UV region of the spectra were observed (Fig. 1A). The second deprotonation step ($[HA] \rightarrow [A]^-$) was accompanied by a small redshift and slight decrease in intensity of the absorption maximum in the visible region and a decrease in absorption maximum without changes in its position in the UV region of the spectra (Fig. 1B). As can be seen from concentration distribution curves (Fig. 1C) the neutral form of Se-3-AP predominates in the physiological pH range. It should be noted that the determined constants represent macro ionization constants. As shown in Scheme 1, K_{a1} represents the dissociation of the protonated pyridinium unit, while K_{a2}coresponds to deprotonation of the hydrazone nitrogen atom of the selenosemicarbazide moiety. K_{a2} accounts

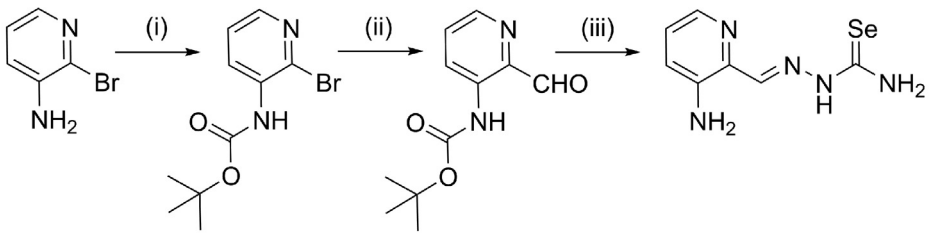

Scheme 1 Three step synthesis of Se-3-AP. Reagents and conditions: (i) sodium bis(trimethylsilyl)amide (1 M, THF), $(Boc)_2O$; (ii) *n*-BuLi, *N*-formylpiperidine; (iii) selenosemicarbazide, conc. HCl, $NaHCO_3$.

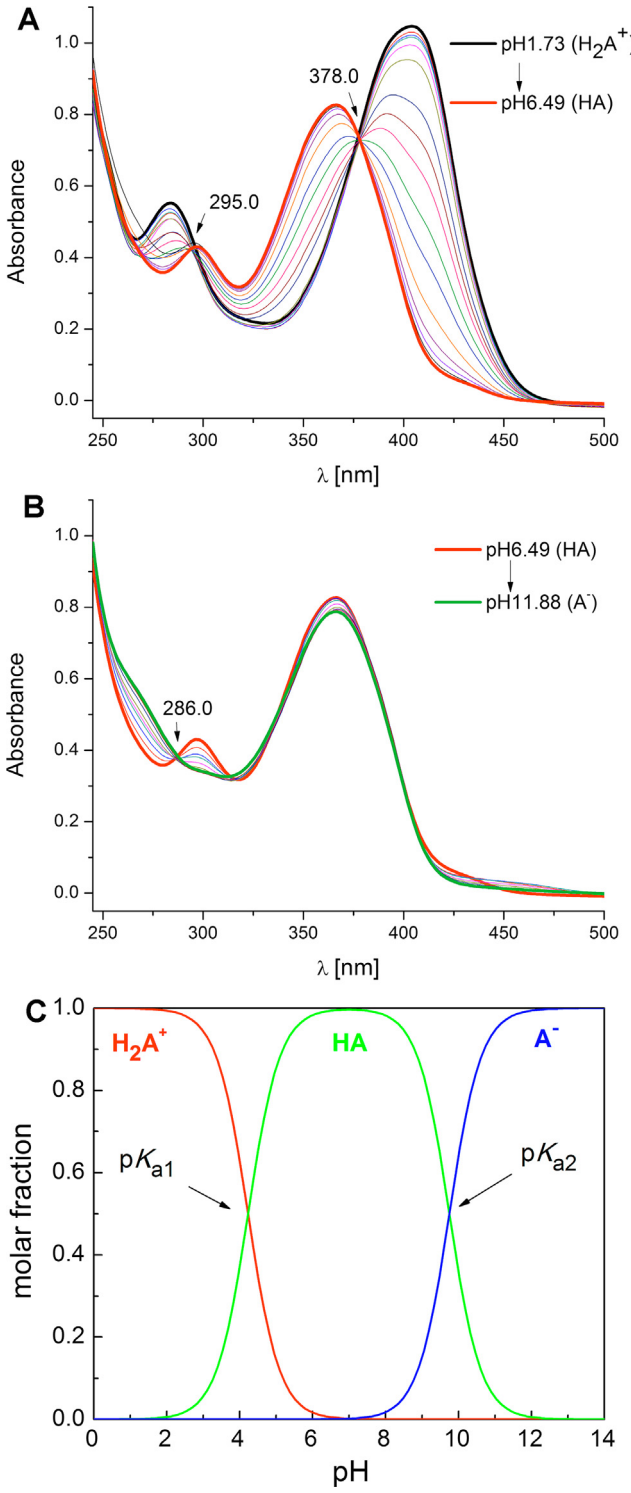

Fig. 1 UV/Vis absorption spectra of Se-3-AP [c = 0.031 mM; t = 25.0 °C, I = 0.10 M (NaCl) in 5% (v/v) DMSO/H2O] recorded in the pH ranges 1.736.49 (A) and 6.4911.88 (B). Spectra of pure H2A+, HA and A– forms and isosbestic points are indicated. Se-3-AP distribution diagram (C).

for different contributions of the selenone tautomer (shown in Scheme 2) and selenenol tautomer (not shown).

The proton donating ability of Se-3-AP and 3-AP was assayed using a protocol for the determination of radical scavenging activity, the 2,2-diphenyl-1-picrylhydrazyl (DPPH) method (Prior et al., 2005). IC_{50} values were calculated from the plotted graph of scavenging activity against the concentrations of the samples. IC_{50} is defined as the total antioxidant necessary to decrease the initial DPPH radical concentration by 50%. Vitamin C was used as the reference compound (positive control). The obtained IC_{50} values (in mM) are as follows: 1.13 ± 0.01, 3-AP; 0.107 ± 0.001, Se-3-AP; 0.079 ± 0.002, vitamin C. These results showed that Se-3-AP is one order of magnitude more potent antioxidant than 3-AP.

3.2. Anticancer activities

3-AP and Se-3-AP have been evaluated in terms of their ability to induce cell apoptosis in THP-1 and MCF-7 malignant cell lines. Compounds were added in a range of six concentrations and left on cells for 24 h, afterwards percentages of live and dead cells were determined by means of Annexin V/propidium iodide (PI) dual staining assay. Both, 3-AP and Se-3-AP have proven to be strong inducers of cell death in THP-1 cells but with apparently different activity. Treatment of THP-1 cells with 3-AP administered in a span from 1–100 μM predominantly induced accumulation of double stained events in the quite high percentage already at the lowest employed concentration, with a concentration-dependent increase throughout the concentration range (Fig. 2A, left panel). At the same time, percentages of Annexin V single-stained cells that represent events in the early phase of apoptotic death, has remained at the level of untreated control, while incidence of necrotic cells remained above 10% and in almost all treated samples. Since Annexin V/PI double stained cells can be interpreted as cells in advanced phases of apoptosis or necrosis, the coincidental lack of early apoptotic events clearly indicates that treatment with 3-AP induced a vigorous necrotic response in THP-1 cell line. For that reason 3-AP is considered to possess an unfavorable mode of activity and was not included in further evaluations on this cell line. On the other hand, treatment of THP-1 cells with Se-3-AP in initial range from 1–100 μM also induced a major accumulation of double-stained cells, but those were accompanied by significant percentages of cells at the initial phase of apoptotic death (data not shown). Considering the incidences of cell death were too high in the span of applied concentrations describing only the top plateau of the concentration–response sigmoidal curve so that ED_{50} concentration could not be determined, it was necessary to decrease concentration range of Se-3-AP on THP-1 cells half the way down to 0.5–30 μM. As represented in Fig. 2B, treatment with Se-3-AP gradually and concentration-dependently increased percentages of cells in early and late phases of apoptosis, whereas incidence of necrosis was preserved on the level of untreated control. Those data described sigmoidal concentration-response curve with a wide slope while the top plateau begins at the concentration of 30 μM (Fig. S10A, Supplementary data). Such a curve is characteristic of a drug which dose can be accurately titrated to achieve a desired outcome while easily avoiding any toxic effect.

Treatment of MCF-7 cells with 3-AP (1–100 μM) resulted in poor frequency of cell death while the majority of those events were also in the process of necrotic death (Fig. 2A, right panel). On the contrary, Se-3-AP on the same cell line induced strong apoptotic response with concentration–response curve nicely defined within applied range of 1–100 μM (Fig. 2C

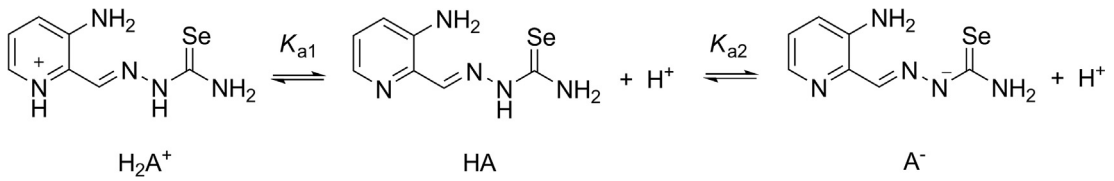

Scheme 2 Proteolytic equilibria of Se-3-AP in aqueous media. HA, as neutral form of Se-3-AP, is represented in one tautomeric form, while all tautomers coexist in solution.

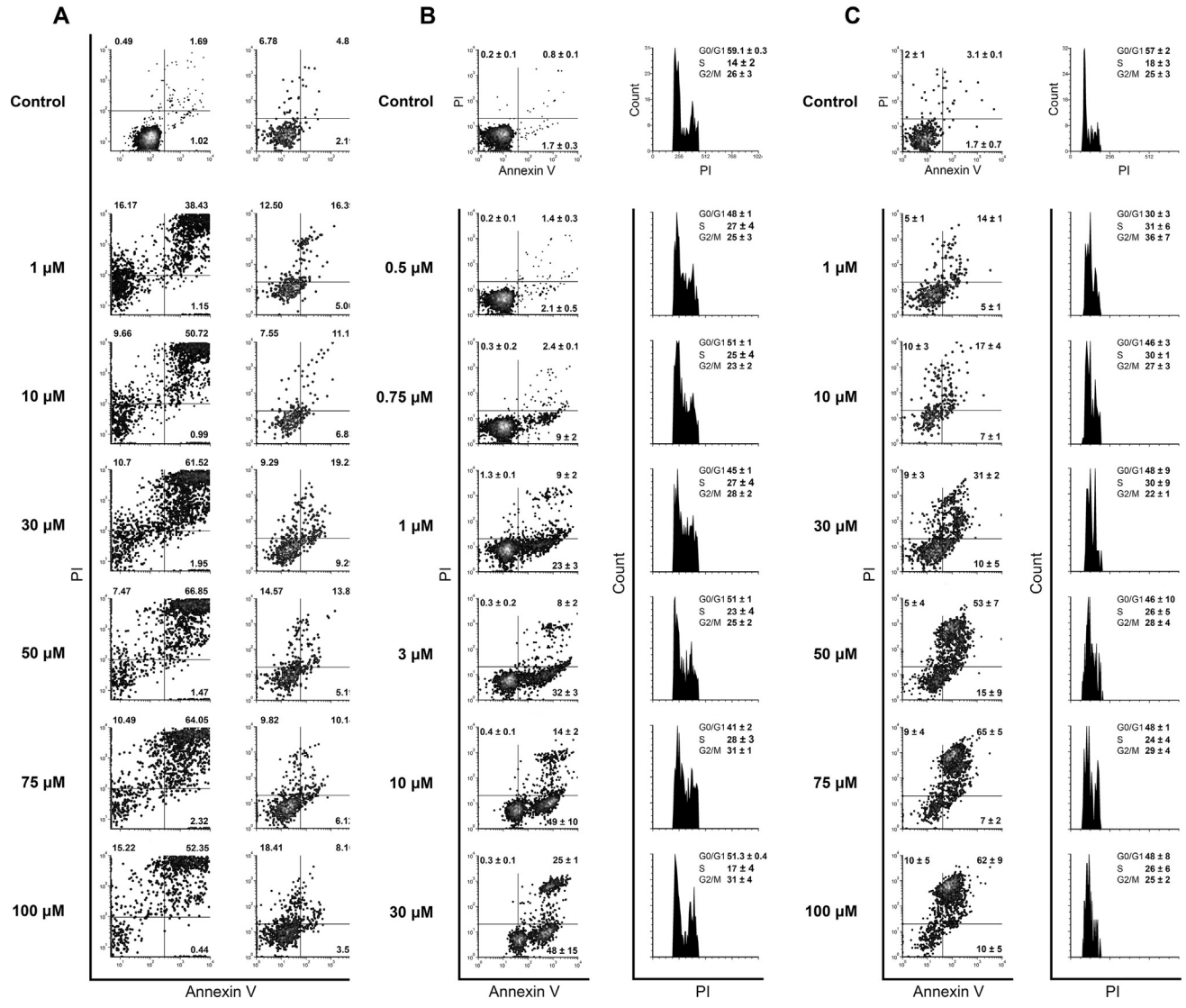

Fig. 2 (A) Types of cell death in THP-1 (left panel) and MCF-7 cells (right panel) treated with 3-AP. Results are represented as percentages of stained cells from a single experiment considering the replicates have not been acquired due to high toxicity or lack of activity. (B) Types of cell death (left panel) and changes in cell cycle distribution (right panel) in THP-1 cells treated with Se-3-AP. (C) Types of cell death (left panel) and changes in cell cycle distribution (right panel) in MCF-7 cells treated with Se-3-AP. Types of cell death in each experiment were determined after 24 h incubation by Annexin V/PI double staining. Changes in cell cycle distribution on both cell lines have been assessed on the same cell samples used for Annexin V/PI read out. Incidences of cells found in G0/G1, S and G2/M phases were determined according to non-treated control population. Results in (B) and (C) are expressed as the mean ± SD (n = 2 independent replicates).

and Fig. S10B Supplementary data). However, concentration–response curve, which describes activity of Se-3-AP on MCF-7 cell line, distinguishes from that defined for THP-1 cells by the slope positioned within a narrowed concentration span, while the top plateau started already from the concentration of 50 μM (Fig. S10A, Supplementary data).

Changes of cell distribution within phases of mitotic division in THP-1 cells caused by the treatment with Se-3-AP have shown moderate concentration-dependent variations (Fig. 2B, right panel). Moderate accumulation of dividing cells at the G1-to-S phase of the cell cycle was evident up to the concentration of 3 μM, when a gradual decrease in percentage of cells at the S phase was recorded. Thus in the samples treated with Se-3-AP at 30 μM incidence of cells at the S phase returned to the level of non-treated control accompanied with discrete accumulation of cells at the G2/M phase. Gathering of cells at the S phase was also found in the MCF-7 treated samples (Fig. 2C, right panel). However, Se-3-AP at concentration of 1 μM aroused formation of S-to-G2 arrest that already at the next concentration level of 10 μM shifted into cell collecting at the G1-to-S phase. Considering necrosis was the dominant form of cell death in THP-1 cells treated with 3-AP, changes in cell cycle progression were not assessed due to their irrelevance.

Although 3-AP showed weak pro-apoptotic activity in MCF-7 cells, so that what type of changes it induced at 10, 50 and 100 μM only were evaluated (Fig. S11, Supplementary data). Incubation of MCF-7 cells with 3-AP resulted in a slight accumulation of cells at the G2/M phase instead at the G1-to-S that was seen after treatment with Se-3-AP (Fig. 2B and C).

In order to evaluate the role of caspase activation in apoptotic death of THP-1 and MCF-7 cells induced by the treatment with Se-3-AP, cells were incubated with this compound at the ED_{50} concentration with and without the presence of the pan-caspase inhibitor *N*-benzyloxycarbonyl-Val-Ala-Asp(O-Me) fluoromethyl ketone (Z-VAD-fmk). After 6 h of treatment, cells were analyzed by means of Annexin V/PI dual staining method, and changes in incidences of apoptotic and necrotic events between samples treated with Se-3-AP alone and co-incubated with Z-VAD-fmk were computed. As represented in Fig. 3A, the addition of pan-caspase inhibitor almost completely inhibited apoptosis induced by Se-3-AP in both cell lines. Nevertheless, the lack of caspase activity induced treated cells to necrosis. This result demonstrates that apoptosis in THP-1 and MCF-7 cells was highly dependent upon caspase activation. The only dissimilarity observed between those two cell lines concerns different caspase-dependency of apoptotic death initiation, which may indicate on possibility that Se-3-AP in MCF-7 cell also can trigger caspase-independent apoptosis.

Further, we wanted to determine which caspase pathway was primarily activated in THP-1 and MCF-7 cells by the treatment with Se-3-AP. For that reason, cells were treated with Se-3-AP at its ED_{50} concentration and assayed after 6 h incubation for caspase-8 and -9 activities. Results are presented as average percentage of cells that express activated either caspase-8 or caspase-9 alone, and an average percentage of cells that express both activated caspases (Fig. 3B). In non-treated THP-1 samples, a basic level of activated caspase-9 exits (5.9 ± 0.3% of cells), while percentages of cells with activated caspase-8 only or both caspases were very low (0.5 ± 0.4% and 0.4 ± 0.3%, respectively). Quite the opposite, percentage of non-treated MCF-7 cells with primarily activated caspase-8 (3.3 ± 0.6%) and both activated caspases (3 ± 1%) dominated over activation of caspase-9 (0.6 ± 0.1%).

For Se-3-AP treated THP-1 samples high but non-significant increase in percentage of cells positive for activated caspase-9 only was found (20 ± 4%), whereas a high level of significance was determined comparing cells which displayed activated form of both caspases. Results of this assay definitely reveal that the dominant mechanism of apoptosis triggered by Se-3-AP in THP-1 cells involves activation of intrinsic apoptotic pathway, whereas activation of caspase-8 arises as a result of cross-talk between these two apoptotic pathways. Activation of caspase-9 was the mainstream event in MCF-7 cells too. However, here the cross-talk between intrinsic and extrinsic apoptotic pathways evidently did not play any important role in signal transduction during apoptotic process.

Capacity of Se-3-AP to induce generation of mitochondrial superoxide radicals ($O_2^{-\cdot}$) has been evaluated on both cell lines. Percentages of THP-1 and MCF-7 cells positive for mitochondrial $O_2^{-\cdot}$ have been evaluated by MitoSox Red in cells after 6 h incubation with Se-3-AP [50 μM]. Results were analyzed with regard to following parameters: percentage of $O_2^{-\cdot}$-positive cells, and median fluorescence intensity (MFI) determined for $O_2^{-\cdot}$-positive subpopulation of cells expressed in arbitrary units (AU). MFI is relevant of the quantity of generated $O_2^{-\cdot}$ per cell. Percentages of $O_2^{-\cdot}$-positive cells in non-treated controls, THP-1 and MCF-7 cell lines are different in their basal potential for generating mitochondrial $O_2^{-\cdot}$ (5.2 ± 0.7 AU and 20 ± 7 AU for THP-1 and MCF-7 cells, respectively), while MFI values for those controls were almost the same (Fig. 4A and B). After addition of Se-3-AP to THP-1 cells, percentage of $O_2^{-\cdot}$ positive cells increased three fold, but the median amount of generated $O_2^{-\cdot}$ per cell remained at the level of non-treated control. On the contrary, treatment of MCF-7 cells with Se-3-AP doubled the percentage of $O_2^{-\cdot}$-generating cells, whereas the amplitude of superoxide production per cell was significantly higher than in control population. This result demonstrates the phenotype-specific response to Se-3-AP regarding mitochondrial$O_2^{-\cdot}$ generation.

Following the insight that treatment with Se-3-AP significantly increased mitochondrial $O_2^{-\cdot}$ production in MCF-7 cells only, together with the fact that activation of intrinsic apoptotic pathway was the executive in the process of their apoptotic death, it was decided to evaluate the loss of mitochondrial transmembrane potential (MTP) in this cell line. Evaluation of MTP dissipation has been assessed after 6 h incubation of MCF-7 cells with Se-3-AP (c = 50 μM). Chosen concentration being the same as for determination of mitochondrial $O_2^{-\cdot}$ production, allowing an unbiased estimation whether generation of $O_2^{-\cdot}$ was the main cause for activation of intrinsic apoptotic pathway. As seen in Fig. 4C, almost all the cells in non-treated controls with altered MTP were additionally single-stained with 7-AAD indicating necrotic death. Compared to control, treatment with Se-3-AP induced about a twofold increase in percentage of cells with dissipated MTP, whereas regarding their staining with Annexin V and 7-AAD a similar distribution was recorded as in non-treated control. Majority of Se-3-AP-treated cells that showed loss of MTP were 7-AAD single-stained, while only few of them were labeled with Annexin V alone. Considering the short incubation time and significantly small percentage of cells found in early apoptosis (Annexin V-single stained events), necrosis remains the main way leading to cell death.

The treatment impact on MCF-7 3-D spheroids was monitored in regard of changes in size and morphology. Insufficient mass transport of oxygen, nutrients and metabolites through cellular barriers of spheroidal structure clearly distinguishes three concentric zones: necrotic core (dark sphere located in

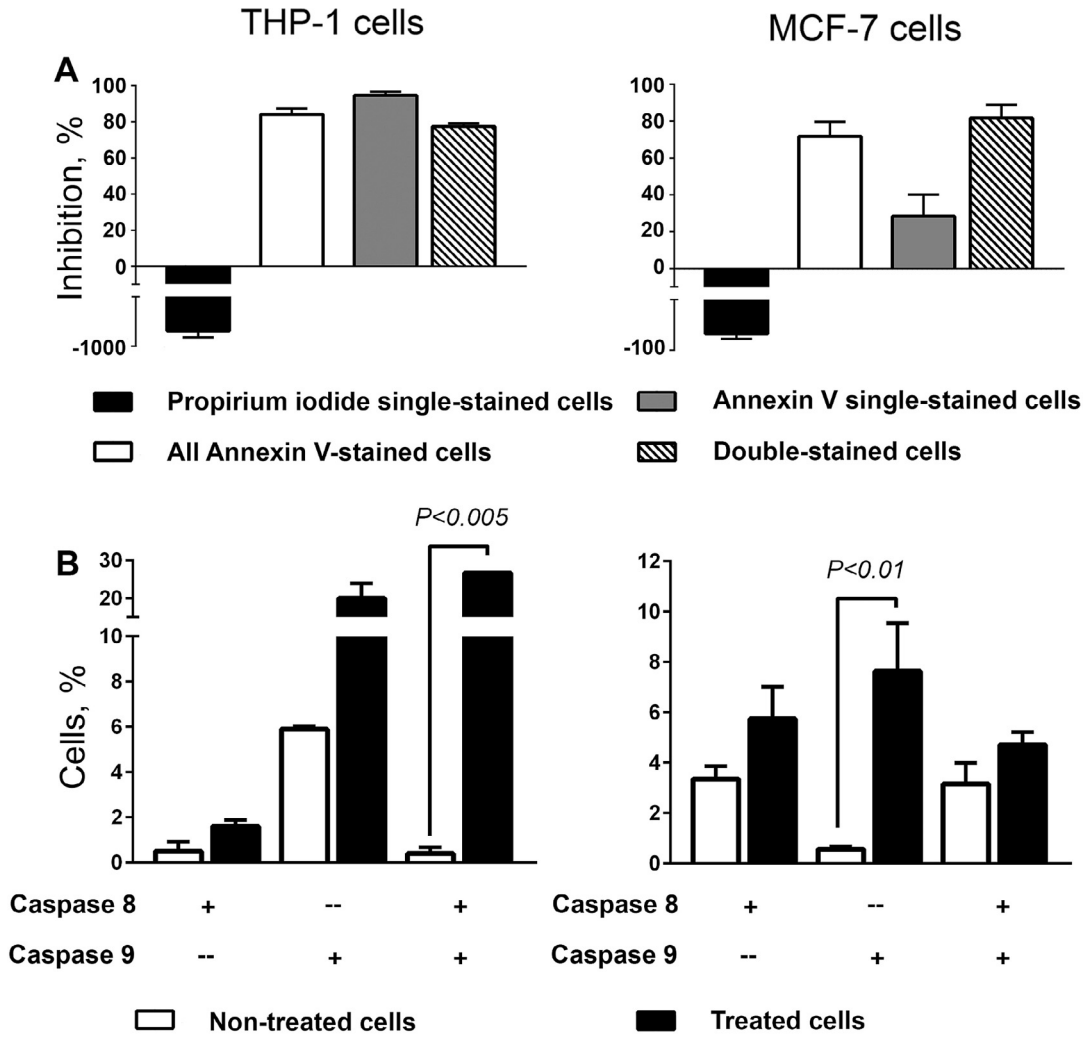

Fig. 3 (A) Impact of pan-caspase inhibitor Z-VAD-fmk on incidences of apoptotic and necrotic cell deaths in THP-1 and MCF-7 cells treated with Se-3-AP applied at ED50 concentration. (B) Percentage of THP-1 and MCF-7 cells with activated caspase-8 or/and caspase-9 due to treatment with Se-3-AP applied at ED50 concentration. All results are presented as the mean ± SD (n = 3 independent replicates).

the center of 3-D culture consisting of dead cells), quiescent zone (transparent dark gray rim that surrounds necrotic core, consisting of living non-dividing cells) and the proliferating zone (transparent border located on the outer edge). For non-treated spheroids, sizes and mutual ratio of those zones will alter over days of incubation. Thus, due to the expansion in size, necrotic core will get bigger while quiescent zone will thin and shoves towards the very edge of the sphere (Fig. 5A). Increase in size of control spheroids was 2.3 ± 0.1-fold in 8 days (Fig. 5B). Activity on 3-D culture was evaluated for Se-3-AP applied in 3 concentrations (1, 10 and 100 μM). Treatment with 1 μM is not presented due to lack of activity. Se-3-AP at 10 μM caused a delay in growth of MCF-7 spheroids. Regression in size regarding volumes on the day 0 has not been achieved, but those spheres were significantly smaller compared to non-treated controls (Fig. 5B). Considering proportion of the 3 structural zones, there were no major differences observed comparing non-treated and spheres treated with 10 μM (Fig. 5A). On day 6, quiescent zone almost completely merged with the necrotic core barely distinguished on high magnification microscopy (data not shown). Finally, proliferation zone was completely obliterated on day 8, forming a crispy shaped brim as an indication of accelerating cell death. When compared to 10 μM, treatment with Se-3-AP at 100 μM restrained spheroidal growth efficiently (1.0 ± 0.2-fold versus 1.4 ± 0.2-fold computed on day 8 for spheres treated with 100 and 10 μM, respectively). Morphological changes of spheroids in this concentration-treated group were far more striking (Fig. 5A). Starting from day 2, quiescent zone was gradually getting darker, accompanied with progressive contraction of proliferation zone. On day 4, the proliferation zone was barely detectible, while on the next day their edges became shredded. It is interesting to note that necrotic core was easy to distinguish, with the quiescent zone preserved until the end of the treatment.

The SmartFlare technology used here allows us the detection of gene expression in living cells with opportunity for single-cell profiling. In this study, expression levels of octamer-binding transcription factor 4 (Oct-4) was monitored. Oct-4, has been found reactivated in many cancers concomitantly with a reversion of cell phenotype from a highly differentiated state to a highly undifferentiated state, which

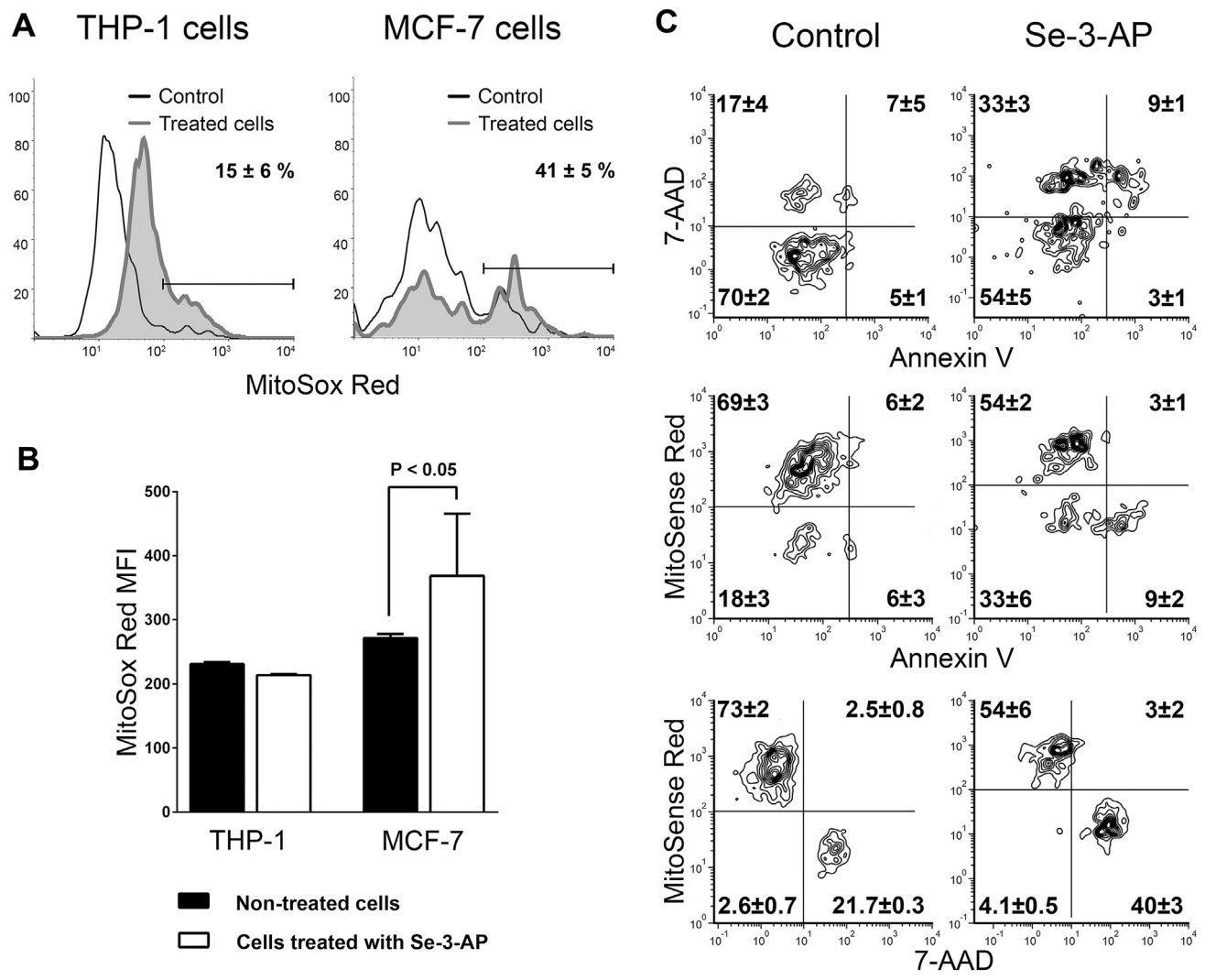

Fig. 4 (A) Percentages of THP-1 and MCF-7 cells positive for mitochondrial $O_2^{\cdot-}$ after 6 h treatment with Se-3-AP [50 μM], as determined by MitoSox Red. Results are presented as the mean ± SD (n = 3 independent replicates). (B) MFI of MitoSox Red-stained cells giving a median quantity of produced $O_2^{\cdot-}$ per cell. Statistical significance has been determined by unpaired *t* test with Welch's correction (n = 3 independent experiments). (C) Changes of mitochondrial membrane potential in MCF-7 cells after 6 h treatment with Se-3-AP [50 μM], as determined by MitoSense Red. Results are presented as the mean ± SD percentage of cells discriminated according to labeling by MitoSense Red, Annexin V and 7-AAD (n = 2 independent replicates).

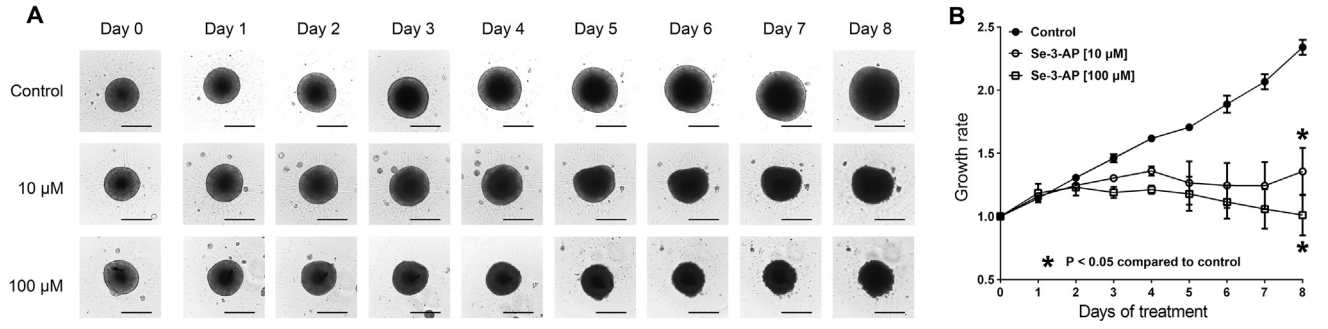

Fig. 5 (A) Changes in size and morphology of MCF-7 3-D cultures induced by Se-3-AP applied at concentrations of 10 and 100 μM over the 8-day treatment. Images were acquired daily starting from the day 0 with Celigo imaging cytometer using Celigo software. Scale bar: 200 μm. (B) Growth rates of MCF-7 3-D cultures, non-treated and treated with Se-3-AP applied at concentrations of 10 and 100 μM. Results are expressed as the mean ± SD (n = 3 independent replicates). Statistical significance has been determined by means of Kruskal-Wallis test followed by unpaired *t* test with Welch's correction as posttest.

contributes to cancer development and aggressivity. Knowing the contribution of Oct-4 in development of resistance and tumor recurrence after applied treatment, it is important to monitor its expression so to follow the putative aggressivity of the leftover cells after chemotherapy (Emhemmed et al., 2017). Results of Oct-4 detection should be considered in respect to few important remarks. Assessment of Oct-4 expression has been estimated in the living cells only, a population gated on forward scatter versus side scatter dot plot. Size of this subpopulation varied between from 10 to 20% of all acquired cells in our samples. In terms of previously reviewed results of morphological analysis of non-treated and treated spheroids on day 8, it is obvious that such a low percent of viable cells was due to a massive necrotic core found in control samples, and from accelerated cell death induced by applied treatments. In general, majority of vital cells within spheroids are situated in quiescent zone, consisted of cells in state of dormancy, and in the proliferating zone.

In non-treated spheroids, a high percentage of cells displayed active transcription of Oct-4 gene after 16 h of incubation with SmartFlare detection probe (Fig. 6). Treatment with Se-3-AP induced a noteworthy down-regulation of Oct-4 expressing cells in concentration-dependent manner (Fig. 6A). While 10 μM Se-3-AP abolished Oct-4-transcription in almost 50% of cells, treatment with 100 μM induced a reduction up to 75%. Additionally, according to MFI values, significant decrease in median Oct-4 mRNA transcripts per cell was achieved only in spheroids subjected to Se-3-AP at 100 μM (Fig. 6B). Those results reveal that treatment with 100 μM Se-3-AP stimulates a strong phenotype reprogramming of MCF-7 cells.

3.3. Inhibition of Cu-mediated DNA damage

In order to compare ability of Se-3-AP and 3-AP in inhibition of Cu(I)-mediated oxidative DNA damage, the assay developed by Battin et al. (2011) was employed. As it can be seen in Fig. 7, both Se-3-AP and 3-AP showed the ability to mitigate oxidative DNA damage caused by hydroxyl radical generated in the Fenton reaction. Agarose gel electrophoresis of pUC19 DNA plasmid alone revealed that almost all DNA was in a supercoiled form (SC), with nicked form (NC) only in traces, while linear form (L) was not evident (Fig. 7, lanes 1). Hydrogen peroxide alone (Fig. 7, lanes 2) and in a combination with 3-AP and Se-3-AP (Fig. 7A lane 3 and Fig. 7B lane 3, respectively) did not induce any damage on plasmid DNA, since proportion of SC and NC forms remained unchanged in respect to native plasmid DNA. However, when plasmid DNA was incubated with Cu(I) and H_2O_2 (reactive mixture), the SC

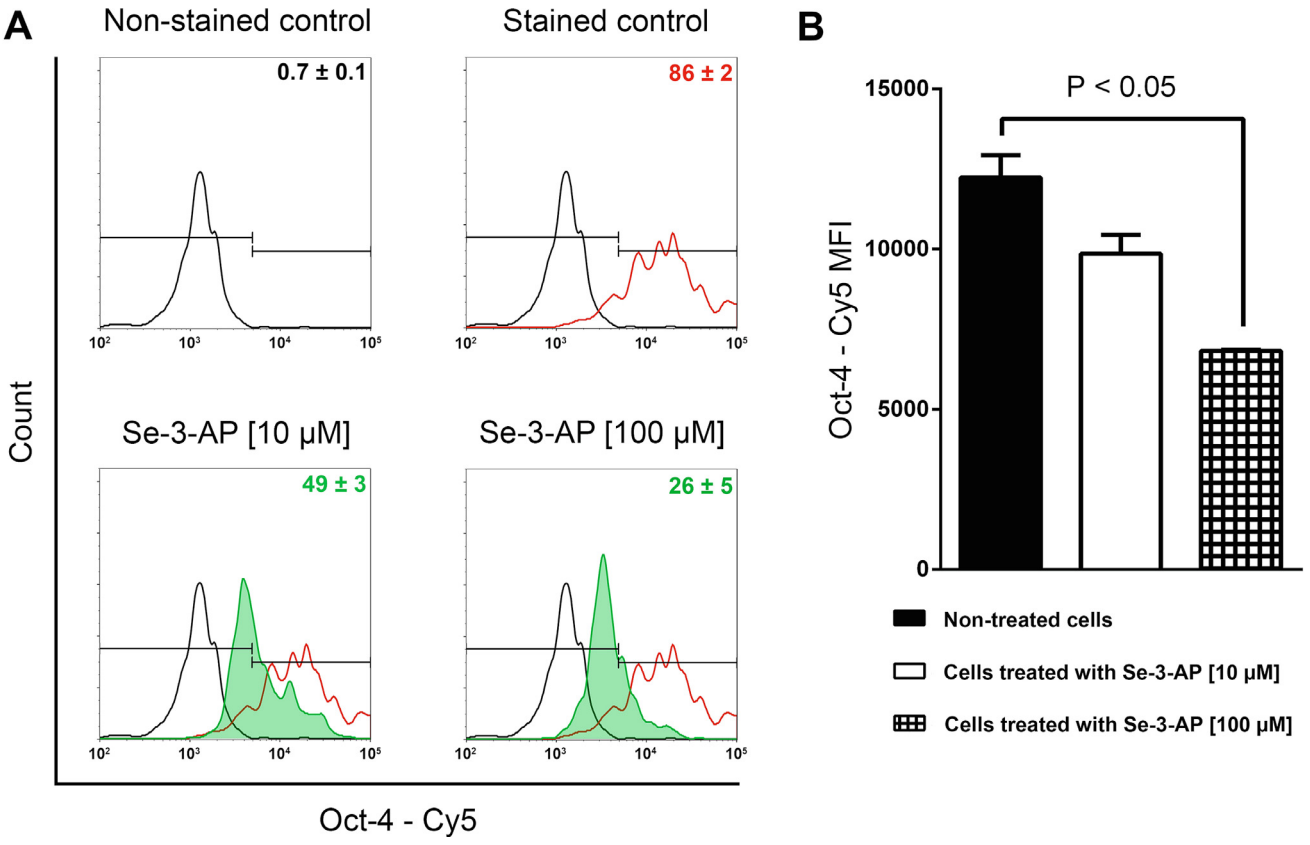

Fig. 6 (A) Histogram of population of cells positive for RNA transcripts of Oct-4 mRNA in MCF-7 3-D cell cultures afterwards 8-day treatment with Se-3-AP applied at 10 and 100 μM (green), and non-treated controls from the same experiment (red). RNA transcription was determined by SmartFlareRNA detection probe. Results are expressed as the mean ± SD (n = 3 independent 3-D replicates). (B) MFI (AU) of Oct-4 expression indicating on median quantity of Oct-4 RNA transcripts per cell. Results are expressed as the mean ± SD (n = 3 independent 3-D replicates). Statistical significance has been determined by Kruskal-Wallis test, with unpaired *t* test with Welch's correction as posttest.

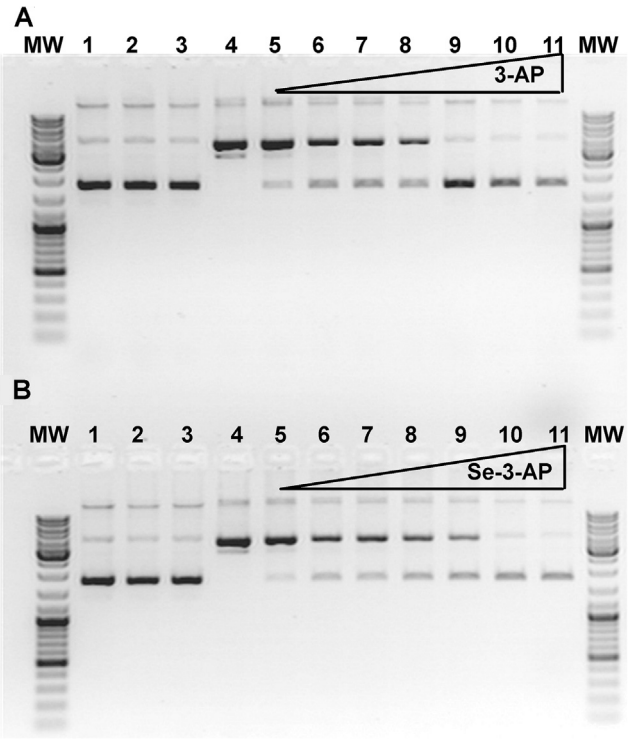

Fig. 7 Agarose gel showing a reduction in oxidative DNA damage with increasing concentration of 3-AP (A) and Se-3-AP (B). Lanes: (MW) GeneRuler DNA 0.1–10.0 kb ladder mix; (1) plasmid DNA; (2) DNA + H_2O_2; (3) DNA + 3-AP/Se-3-AP + H_2O_2; (4) DNA + Cu(II)/ascorbate + H_2O_2; (5–11) same as lane 4 with increasing concentration of 3-AP/Se-3-AP: 0.1, 1, 5, 10, 50, 100 and 1000 mM, respectively.

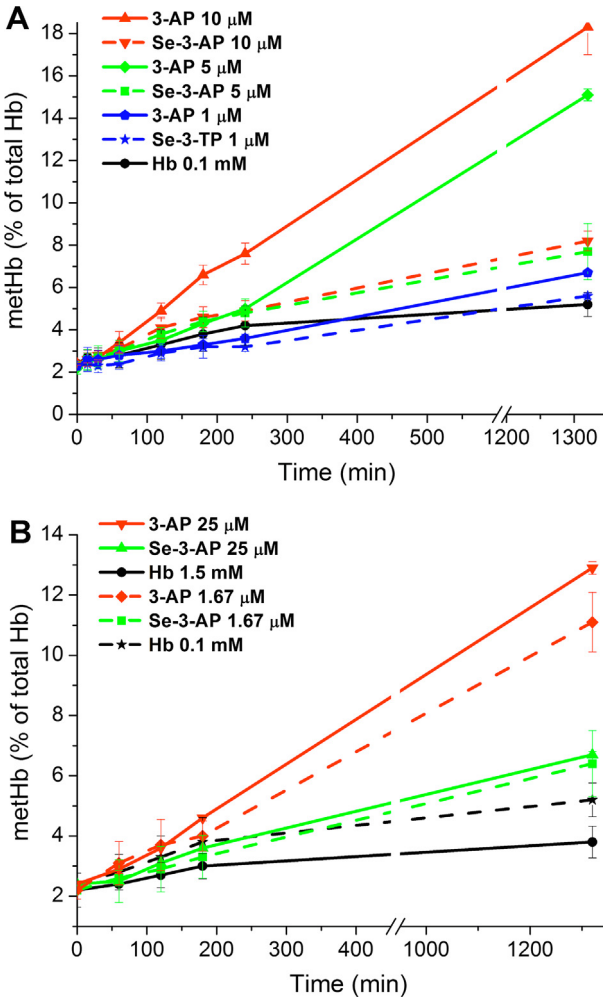

Fig. 8 MetHb formation induced by 3-AP and Se-3-AP. (A) RBC lysates [total Hb concentration 0.1 mM in 0.1 mM phosphate buffer saline (PBS) pH 7.4] was incubated without (control) and with Se-3-AP or 3-AP (10, 5 and 1 μM). (B) RBC lysates (total Hb concentrations of 1.5 and 0.1 mM in 0.1 mM PBS pH 7.4) were incubated without (control) and with sixty times lower concentration of Se-3-AP or 3-AP (25 μM or 1.67 μM, respectively). Maximum incubation period was 1320 min at 37 °C. Results are means ± S.D. for three experiments.

form completely disappeared, while NC became dominant with L form found in traces (Fig. 7, lanes 4). As it can be seen in Fig. 7 (lanes 5–11), when 3-AP or Se-3-AP were added to the reactive mixture, concentration-dependent shifts in ratio of plasmid DNA forms were achieved.

3.4. In vitro metHb formation

To assess the effect of Se-3-AP on in vitro metHb formation compared to 3-AP, a solution of Hb (0.1 mM), obtained from red blood cells (RBC) lysate of healthy human donor, was incubated without (control) and with Se-3-AP and 3-AP (10, 5 and 1 μM) for up to 22 h at 37 °C. The content of metHb in the incubation mixtures was determined by the standard method (Winterbourn and Carrell, 1977). The results are shown in Fig. 8A. MetHb fraction in non-treated controls at 0 min was 2.4%, which is in the range for metHb values determined in healthy individuals (0–3%) (He and Carter, 1992). Results showed that metHb concentration increased time- and dose-dependently in the samples treated with Se-3-AP and 3-AP (Fig. 8A). 3-AP at concentrations 10 and 5 μM induced statistically significant ($p < .05$) increase of metHb content compared to the control after 60 and 240 min of incubation, respectively. After 22 h of incubation 10 μM concentration of 3-AP induced about three times higher metHb content, compared to the control. In the samples treated with Se-3-AP (5 and 10 μM), statistically significant increase in metHb concentration ($p < .05$) was reached only after 22 h of incubation. Also, Se-3-AP and 3-AP (1 μM) prevented metHb formation over the first 240 min of incubation period, while only 3-AP (1 μM) after 22 h led to significantly ($p < .05$) increased metHb formation, compared to the control.

Since oxyHb concentration in the blood of healthy individuals is 15–25 times higher than its concentration in this experiment, to assess the metHb formation in circumstances that are more physiological, 1.5 mM of oxyHb was incubated without (control) and with Se-3-AP and 3-AP (25 μM) for up to 22 h at 37 °C. Results of this experiment were compared to those when 0.1 mM oxyHb was incubated without (control) and with Se-3-AP and 3-AP (1.67 μM), thus in both settings molar ratio of oxyHb: Se-3-AP/3-AP was 60: 1 (Fig. 8B). With elevated Hb concentration in the incubation mixture, effects of Se-3-AP and 3-AP were more pronounced and an increase of

metHb content after 180 min of incubation was noticed. Both concentrations of 3-AP (25 and 1.67 μM) led to statistically significant ($p < .05$) rise in metHb content compared to corresponding controls after 120 min, while Se-3-AP (25 μM) achieved significantly higher genesis of metHb only after 22 h of incubation compared to the corresponding control (6.7 ± 0.1% and 3.8 ± 0.5%, respectively). After 22 h of incubation, for all concentrations of Se-3-AP and all molar ratios of oxyHb: Se-3-AP, the obtained metHb content was always below 8.5% (Fig. 8).

3.5. Interaction with HSA

UV/vis and fluorescence spectroscopy were used to study interaction of Se-3-AP with HSA. UV/vis spectra of Se-3-AP with increasing amounts of HSA (Se-3-AP/HSA molar ratios from 1: 0.06 to 1: 0.5) showed a blue λ_{max} shift (from 373 to 367 nm, Fig. 9A). Interaction between HSA and Se-3-AP lead to changes in the absorption spectra of Se-3-AP upon its binding to HSA. The changes in fluorescence emission spectra of HSA with increasing amount of Se-3-AP (Se-3-AP/HSA molar ratios from 1.5: 1 to 15: 1) are shown in Fig. 9B. The excitation wavelength was 280 nm, at which both Trp214 and Tyr residues emit fluorescence. In spite of the presence of 18 Tyr residues in HSA molecule (He and Carter, 1992), the HSA intrinsic fluorescence is dominated by single Trp214 in subdomain IIA (Lakovicz, 2006). The binding of Se-3-AP to HSA resulted in fluorescence quenching at λ_{em} (340 nm). In the presence of Se-3-AP, the intrinsic fluorescence decreased in a concentration-dependent manner, suggesting that Se-3-AP interact with HSA. A blue shift in the emission maximum wavelength occurred, indicating that the microenvironment around Trp214 is altered into a more hydrophobic as the HSA–Se-3-AP adduct is formed (Li and Yang, 2015).

Fluorescence quenching data were further processed in order to perform more detailed characterization of Se-3-AP–HSA binding. The obtained Stern–Volmer quenching constant (K_{sv}), the quenching rate constant (k_q), the effective quenching constant for the accessible fluorophores (K_a), the fraction of accessible fluorophore (f_a), thermodynamic binding parameters, association constants (K_b) and number of binding sites (n) of HSA are given in Table 1 and Figs. S12–S15 (Supplementary data). Obtained values for K_{sv} decrease as temperature increases. The values for K_{sv} indicate that the quenching mechanism is static. The obtained k_q values are three orders of magnitude higher than the limiting diffusion rate constant of the biomolecule ($\sim 10^{10}$ M^{-1} s^{-1}), indicating a static type mechanism of fluorophore quenching (Li et al., 2014). The K_a is inversely correlated with temperature, which is in accordance with K_{sv} temperature dependency. The obtained values for ΔH and ΔS are –5.70 kJ mol^{-1} and 88.56 kJ mol^{-1}, respectively. At all three temperatures obtained values for n were close to 1.

To further examine the binding of Se-3-AP to HSA, the docking in ibuprofen binding site of HSA was performed. Molecular docking gave conformations with the lowest binding energy of –5.5 kcal mol^{-1}, *i.e.* 92 μM. There is an aromatic interaction formed between Trp214 and aromatic ring of Se-3-AP. Selenium atom also forms Se···π interactions with the same amino acid residue. Hydrogen bonds with Ser464 and Glu450 are formed *via* selenoamide group (Fig. 10).

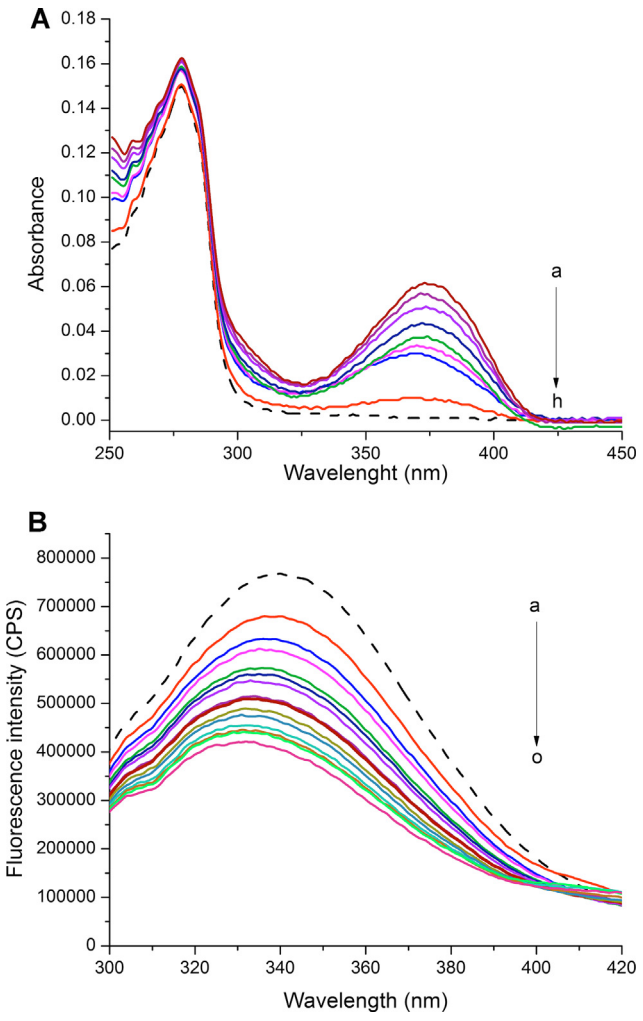

Fig. 9 (A) Changes in UV/vis absorption spectra of Se-3-AP (64 μM in 100 mM PBS pH 7.4) upon addition of HSA in the following molar ratios Se-3-AP/HSA: (a) 1:0.06; (b) 1:0.07; (c) 1:0.08; (d) 1:0.1; (e) 1:0.125; (f) 1:0.17; (g) 1:0.25; (h) 1:0.5. UV/vis absorption spectrum of HSA (4 μM) is represented with a dashed line. (B) Changes in fluorescence emission spectra of HSA (0.125 μM in 100 mM PBS pH 7.4) upon addition of Se-3-AP in the following molar ratios HSA/Se-3-AP: (a) 1:0; (b) 1:1.5; (c) 1:3; (d) 1:4; (e) 1:5; (f) 1:6; (g) 1:7; (h) 1:8; (i) 1:9; (j) 1:10; (k) 1:11; (l) 1:12; (m) 1:13; (n) 1:14; (o) 1:15.

3.6. Acute lethality assay

Acute toxicity of 3-AP and Se-3-AP was tested on brine shrimp *Artemia salina* after 24 h incubation and results are expressed as LC_{50} values. DMSO, as negative control, did not cause changes in viability of treated nauplii. Treatment with $K_2Cr_2O_7$, as positive control, induced high incidence of lethality (LC_{50} = 248.14 ± 16.85 μM). Nauplii revealed different level of sensitivity toward 3-AP and Se-3-AP, where LC_{50} values are 563.41 ± 21.35 and 867.27 ± 19.78 μM, respectively. While LC_{50} for 3-AP was found to be only 1.5-fold higher compared to LC_{50} of $K_2Cr_2O_7$, the concentration of Se-3-AP has to be three times as that of $K_2Cr_2O_7$ to achieve the death in a half of treated nauplii.

Table 1 The Stern–Volmer quenching constant (Ksv), the quenching rate constant (kq), the effective quenching constant for the accessible fluorophores (Ka), the fraction of accessible fluorophore (*f*a), the change in the Gibbs free energy (ΔG), association constants (Kb) and number of binding sites (n) of HSA at three temperatures. Results of binding of Se-3-AP to HSA obtained using the modified Stern-Volmer plot; thermodynamic parameters of binding are calculated using the Van't Hoff equation.

T (K)	$K_{sv} \times 10^5$ (M^{-1})	$k_q \times 10^{13}$ (M^{-1} s^{-1})	$K_a \times 10^5$ (M^{-1})	f_a	ΔG (kJ mol^{-1})	$K_b \times 10^5$ (M^{-1})	n
293	4.27 ± 0.10	6.02	4.31 ± 0.02	0.893	−31.65	4.44 ± 0.15	1.049
298	4.08 ± 0.06	5.75	4.19 ± 0.04	0.862	−32.09	4.15 ± 0.07	1.044
310	3.87 ± 0.03	5.46	4.03 ± 0.08	0.833	−33.15	3.88 ± 0.13	1.048

4. Discussion

Spectroscopic and electrochemical data point out to similarities rather than differences among Se-3-AP and 3-AP. UV/vis spectra of both Se-3-AP and 3-AP showed two absorptions in the region 260–450 nm. These maximums are attributed to $n \rightarrow \pi^*$ transitions of the pyridine ring and chalcogensemicarbazide moiety (Enyedy et al., 2010; Filipovic et al., 2016). Se-3-AP in DMSO solution irradiated at λ_{ex} = 360 nm exhibits maximum at 457 nm in emission spectrum, which is identical to 3-AP (Kowol et al., 2010). ^1H and ^{13}C NMR spectral data indicate very small changes in corresponding chemical shifts of Se-3-AP in comparison to 3-AP (Niu et al., 1998). This is in accord with previously published comparative studies for structurally related selenosemicarbazones and thiosemicarbazones where isosteric replacement of sulfur with selenium did not have strong influence on spectroscopic features of two classes of compounds (Castle et al., 2003; Kowol et al., 2008; Todorovic et al., 2017). The chemical shift of ^{77}Se (Fig. S8) was found at a little higher field in comparison to related 2-formylpyridine selenosemicarbazone (Todorovic et al., 2009). All observed peaks in cyclic voltammograms of Se-3-AP and 3-AP are attributed to the irreversible electrochemical reactions. Values obtained for reduction peaks are similar to values obtained for pyridine based chalcogensemicarbazones containing methyl substituents, but with opposite trends (Kowol et al., 2008). Se-3-AP is slightly weaker acid in the first and stronger acid regarding second dissociation step comparing to 3-AP (Enyedy et al., 2010). Similarly to 3-AP, the neutral form of Se-3-AP predominates in the physiological pH range.

Because selenium and sulfur antioxidants can alleviate oxidative damage, numerous animal and clinical trials have investigated the ability of these compounds to prevent the oxidative stress that is an underlying cause of cancer. Selone (C = Se) and thione (C = S) compounds were recognized as potent antioxidants (Zimmerman et al., 2015). Our previous study of quinoline based non-substituted selenosemicarbazones showed that they had an excellent free radical-scavenging effect, which was greater than that of reference antioxidant vitamin C (Filipovic et al., 2014, 2015). One recent comparative study of free radical scavenging activity of disubstituted seleno- and thiosemicarbazones also confirmed a great free-radical scavenging potential of these classes of compounds, but general conclusion about impact of nature of chalcogen atom on antioxidant activity could not be established (Calcatierra et al., 2015). IC_{50} value obtained for Se-3-AP indicates that it is one order of magnitude more potent antioxidant than 3-AP, with antioxidant activity close to vitamin C.

It was previously demonstrated that rapidly dividing neoplastic cells require the excessive amount of iron, which is the reason for them to express markedly elevated level of transferrin receptors thus facilitating enhanced iron uptake (Hogemann-Savellano et al., 2003; Walker and Day, 1986). Those evidences have raised the attention toward chelating agents that became attractive as a potentially useful treatment against cancer growth. Evaluation of thiosemicarbazones that act as chelating agents revealed cancer cells tend to be more susceptible to their activity compared to normal cells (Kalinowski and Richardson, 2005; Whitnall et al., 2006). 3-AP reduced growth of a panel of 60 cell lines for 50% (IC_{50}) in an average concentration of 1.6 μM (Finch et al., 2000; Knox et al., 2007). In another study, 3-AP achieved IC_{50} concentration of 0.45 μM against human ovarian cystadenocarcinoma cells (41 M) and 0.52 μM on human mammary adenocarcinoma cell line (SK-BR-3) (Enyedy et al., 2011). Furthermore, 3-AP showed high activity against growth of M109 murine lung carcinoma, A2780 human ovarian carcinoma xenograft, hydroxyurea (HU) resistant L1210 leukemia and HU-resistant KB nasopharyngeal carcinoma in vivo models (Cory et al., 1994; Finch et al., 2000). Having ability to cross blood/brain barrier, 3-AP effectively eliminated more than 95% leukemia cells in the brain, which is result comparable to that previously reported for cyclophosphamide (Avery et al., 1990).

Results of clinical trials removed the focus from 3-AP as potentially single effective agent to its role in combination treatments. The best anticancer activity in men 3-AP achieved in combination with fludarabine for the treatment of refractory myeloid malignancies, where this combination demonstrated complete response in 17% patients compared with no response in groups treated with 3-AP or fludarabine alone (Karp et al., 2008). In our study, 3-AP was tested on two heterogeneous cell lines but revealed high activity only against THP-1 leukemia cell line. Here necrosis was a prevailing mode of cell death that is in agreement with its clinically established unfavorable toxicity profile. Quite contrary, current results show that Se-3-AP is a powerful inducer of apoptotic cell death in THP-1 and MCF-7 cell lines, while results of intracellular events and toxicity profiles strongly indicate that 3-AP and Se-3-AP do not share the same mechanism of activity.

The main mechanism of 3-AP activity was defined to be inhibition of RR, an enzyme that supplies monomeric precursors required for DNA replication and repair (Nordlund and Reichard, 2006). In the paper, published by Barker et al.

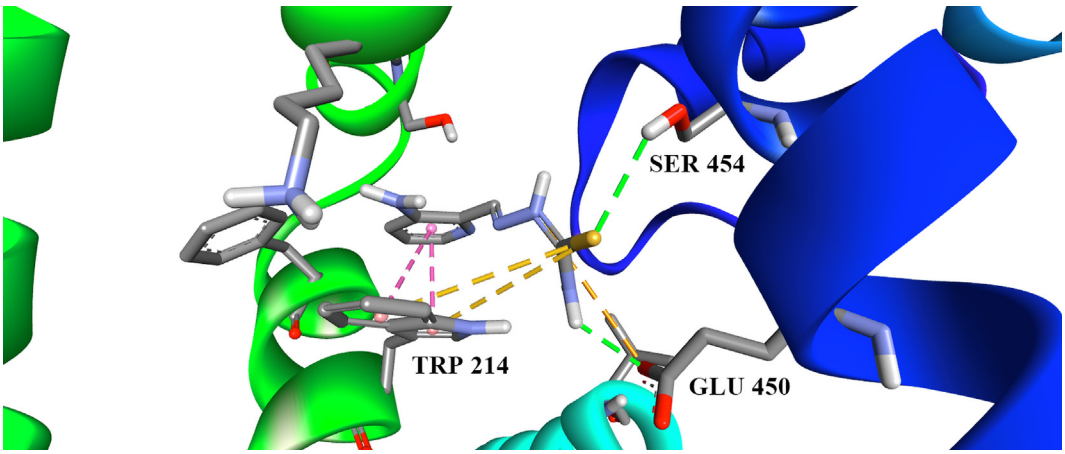

Fig. 10 Se-3-AP docked into ibuprofen binding site of HSA. Green: hydrogen bonds, pink: aromatic interactions; yellow: Se···π interactions.

(2006), minimal disparity between cell cycle changes was found after 16 h treatment with 3-AP in U251 cells (human glioma), DU145 cells (prostate carcinoma) and PSN1 cells (pancreatic carcinoma). In all three cell lines significant accumulation of cell at the G0/G1 phase was seen, accompanied with decreased percentage of S and G2/M phases (Barker et al., 2006). In our study, treatment of MCF-7 cells with 3-AP resulted in a slight accumulation at the G2/M phase instead of the expected G0/G1 block. Current results of cell cycle distribution should be considered in relation with 3-AP poor pro-apoptotic activity revealed in that particular cell line.

Cell cycle changes recorded for Se-3-AP-treated cells in the present study have led to the following conclusions. First, Se-3-AP induced various perturbations within phases of mitotic division amongst treated cell lines, meaning that this compound affected each cell line in a phenotype-specific manner. Thus, while Se-3-AP stimulated moderate accumulation at the S phase in most of THP-1 and MCF-7 samples, concentration that achieved the highest incidence of apoptosis on THP-1 cells did not cause any change within cell cycle distribution, while S-to-G2 block, found for MCF-7 cells, was never seen for THP-1 cells. Second, in both cell lines treatment with Se-3-AP resulted in cell cycle perturbations that altered concentration-dependently. This was most prominent in MCF-7 cells, where Se-3-AP at 1 μM triggered S-to-G2 block, while at the same time did not cause significant percentage of cell death. Increase of Se-3-AP concentration up to 30 μM gradually moved the magnitude toward G1-to-S checkpoint in coincidence with the massive apoptotic response. Such results can be addressed to a concentration-dependent mechanism of activity, which Se-3-AP might performs also independently of cell line phenotype.

It was proposed that redox active Fe(III)/(II)-3-AP complex plays a role in cytotoxicity, with ROS being suggested as ultimately responsible for pharmacologic effects of 3-AP (Shao et al., 2006). However, Aye et al. (2012) revealed that RR is inhibited by Fe(II)-3-AP without ROS formation. Their results were confirmed by other group that demonstrated 3-AP caused pronounced oxidation of mitochondrial thioredoxin-2 and its dependent peroxidase peroredoxin-3 in human cells without effect on cytosolic thioredoxin-1 (Myers et al., 2011). Therefore, the redox stress induced by 3-AP treatment is largely directed at the mitochondria. Relying on literature data on 3-AP activity, we tested capability of Se-3-AP to induce mitochondrial $O_2^{\cdot-}$ production in THP-1 and MCF-7 cell lines. While in non-treated THP-1 samples percentage of $O_2^{\cdot-}$-positive cells was low, the incidence of $O_2^{\cdot-}$ in MCF-7 control samples has been several times higher. There is an interesting positive correlation found between MCF-7 non-treated samples in two different assays, both regarding mitochondrial equilibrium. Precisely, percentage of non-treated MCF-7 cells positive for $O_2^{\cdot-}$ production was almost equal to percentage of non-treated cells positive for dissipated MTP. Comparison of $O_2^{\cdot-}$-positive events between THP-1 and MCF-7 cells in respect to matching controls reveals that treatment with Se-3-AP gained tripled increase in THP-1 cells and doubled increase in MCF-7 cells. However, values of MFI computed for $O_2^{\cdot-}$-positive subpopulation of cells demonstrated that $O_2^{\cdot-}$ production in MCF-7 cells was significantly amplified on a cellular level. Furthermore, strong correlation between results of mitochondrial $O_2^{\cdot-}$ production and altered MTP in MCF-7 samples treated with Se-3-AP was confirmed as well.

Under physiological conditions mitochondrial $O_2^{\cdot-}$ are generated as a result of electron leakage from the respiratory chain and their afterwards reaction with oxygen. Superoxide is further converted to hydrogen peroxide by means of manganese dependent superoxide dismutase (MnSOD) activity, also known as SOD2 (Fukai and Ushio-Fukai, 2011). SOD2 is strategically located to mitochondrial inner membrane, and as a key mitochondrial antioxidant enzyme has a critical role in protection of cell vitality from oxidative stress. Activity of SOD2 is regulated by the deacetylase SIRT3, which expression was recently found to be abolished in 87% of breast cancers (Finley et al., 2011; Tao et al., 2010; Mohan et al., 2016). Papa et al. (2014) showed that the expression of SOD2 is reduced by 50–90% in a panel of breast cancer cell lines compared to human breast epithelial cells (MCF-10A). Thus, antioxidant status in breast cancer cells was maintained owing to mitochondrial fraction of Cu/ZnSOD (SOD1) (Fukai and Ushio-Fukai, 2011). Additionally, MCF-7 cells were shown to have lower expression of mitochondrial SOD1 compared to MDA-MB-231 human breast cancer cell line (Papa et al., 2014). Moreover, recent study revealed that compared to MCF-10A cells, MCF-7 cell line has significantly higher

uncoupled respiration and significantly reduced coupled respiration (Andrzejewski et al., 2014). The mitochondrial respiratory chain uncoupling is the phenomenon that allows the return of proton into the matrix without ATP production. The proton leak lowers potential across the mitochondrial inner membrane, increasing the mitochondrial respiration rate and $O_2^{\cdot-}$ production (Fontanesi, 2015). All these facts are leading to the following conclusions. First, high mitochondrial $O_2^{\cdot-}$ production found in MCF-7 cells after Se-3-AP treatment might relies on distinctive characteristic of the particular cell line, but not on the property of the tested compound. Second, THP-1 cell line was not reported for impaired mitochondrial antioxidant status, thus significantly lower MFI in those cells compared to MCF-7 cell line might resulted from fast and efficient neutralization of superoxide radicals. Those claims are additionally supported by distribution of cells in MitoSOX Red histograms which showed that all THP-1 cells were more or less affected, whereas MCF-7 cells were markedly divided in two subpopulations where the one was strikingly negative for $O_2^{\cdot-}$ whereas the other was highly positive.

Previously published reports indicate that cell death induced by 3-AP was primarily related to activation of caspase-8 induced by ER stress, probably due to formation of ROS, with secondary activated caspase-9 (Alvero et al., 2006; Jimbo et al., 2003). Our results revealed that apoptosis triggered by Se-3-AP in THP-1 cells is highly caspase-dependent and conducted by activation of caspase-9 with secondary activated caspase-8. Katoh et al. (2004) demonstrated that mitochondrial $O_2^{\cdot-}$ can launch caspase-9 activation, which was revealed as the dominant course of apoptosis initiation in both cell lines we have treated in our study. However, comparing intensity of apoptotic induction in THP-1 cells and percentage of $O_2^{\cdot-}$ positive cells, strongly suggests that activation of the intrinsic apoptotic pathway may be rather related to a different incentives.

The inner mitochondrial membrane is the established frontier between mitochondrial inter-membrane space and mitochondrial matrix. It is nearly impermeable to all ions, which in turn allows respiratory chain to build up a proton gradient that is required for oxidative phosphorylation (Mitchell and Moyle, 1965a; Mitchell and Moyle, 1965b). Such electrochemical gradient across the inner membrane forms the basis of the MTP that is of vital importance for cellular bioenergetics (Kroemer et al., 2007). Dissipation of MTP drives a series of consequences that eventually lead to cell death including immediate arrest of mitochondrial ATP synthesis, mitochondrial swelling, an increase of outer mitochondrial membrane permeability with translocation of numerous proteins from mitochondrial inter-membrane space to cytosol that activate the caspase cascade as well as caspase-independent cell death mechanisms (Galluzzi et al., 2008; Galluzzi et al., 2010). In our study, a vast majority of non-treated MCF-7 cells with altered MTP ended in necrosis, whereas the treatment with Se-3-AP raised the percentage of cells with dissipated MTP but did not change the course in type of cell death. Additionally, we found a tight correlation between $O_2^{\cdot-}$ generation and MTP dissipation: percentage of cells positive for $O_2^{\cdot-}$ production was almost equal to percentage of cells with altered MTP, both in non-treated and Se-3-AP-treated samples. With a look back, to clearly segregated subpopulations of $O_2^{\cdot-}$-positive and -negative MCF-7 cells that was discussed above, together with the fact MCF-7 cell line does not represent a single entity but rather large number of individual phenotypes (Comsa et al., 2015), it becomes obvious that Se-3-AP affected MCF-7 cells by a dual mechanisms. The early event is $O_2^{\cdot-}$-dependent and targets susceptible subpopulation of cells driving them into necrotic death. The late event implies triggering of apoptosis as validated at 24 h assessments. The reason $O_2^{\cdot-}$ production and dissipation of MTP did not lead to apoptosis, as well as the mechanism responsible for caspase-9 activation by Se-3-AP treatment of MCF-7 cells remains to be elucidated in further investigations.

After highly promising preclinical data on 3-AP activity, clinical research discovered disappointing results using 3-AP either as a single agent or in combination treatment against solid tumors (Yu et al., 2006). Considering that our study is the first evaluation of Se-3-AP activity where not all aspects of its activity could be investigated, we wanted to assess the effect of Se-3-AP treatment on in vitro derived 3-D tumor model. Spheroid 3-D culture is the unique in vitro tumor model which architecture well mimics in vivo tumor mass with the exception of vasculature and immune system (Grimes et al., 2014). Thus, 3-D models serve as a unique screening platform for drug effectiveness in a function of multiple parameters such as gradient of nutrients, oxygen and metabolites within themselves (Lin and Chang, 2008). Both applied concentrations of Se-3-AP achieved statistically significant delay in growth of MCF-7 spheres compared to control, although none of them induced regression in size of spheroids compared to the first day of evaluation.

SmartFlare technology that was used in our study allows detection of gene expression in living cells with the possibility of single-cell profiling. Since added oligonucleotide probes do not harm cellular integrity and vitality, it is possible to trace changes in gene expression levels due to applied treatment for several targets at the same time (Lahm et al., 2015). Particularly important is that single-cell expression profiling provides information that cannot be deduced from population measurements (Stahlberg et al., 2013; Stahlberg and Kubista, 2014). Oct-4 has been shown as essential for maintaining undifferentiated and pluripotent populations of cells. Its expression profile has been found highly correlated with tumor grade and disease progression (Karoubi et al., 2009; Zhang et al., 2010). Ectopic Oct-4 expression was shown to enhance the features of cancer stem cells in a murine model of breast cancer (Kim and Nam, 2011). Besides that it has important role during tumorigenesis, its stake in development and preservation of drug-resistant phenotype was also confirmed (Wang et al., 2010). Recent studies demonstrated a tight relation between Oct-4 expression and the epithelial to mesenchymal transition (EMT) process (Dai et al., 2013; Kong et al., 2010; Syn et al., 2016). However, it was shown that suppression of Oct-4 expression in MCF-7 cell line promoted invasion and metastasis by induction of EMT (Hu et al., 2011). These contradictory findings suggest that changes in Oct-4 expression can either induce differentiation of cancer cells or to increase their plasticity, meaning that the EMT process may be tightly regulated by endogenous expression of Oct-4. Oct-4 expression rises in residual breast cancer cells that survived the treatment, while the level of its expression is in positive correlation with unfavorable clinical outcome (Magnifico et al., 2009; Saigusa et al., 2009; Zhang et al., 2010). Additionally, hypoxic condition was confirmed to have enhancing influence, with Oct-4 gene is a target of hypoxia inducible factor 2α (Covello

et al., 2006). Our results revealed that Se-3-AP induced significant concentration-dependent down-regulation of Oct4 expression in treated 3-D cultures. Discussing in terms of morphological features, Se-3-AP at 100 μM heavily affected proliferative zone that was unrecognizable from the day 3 of treatment while the quiescent zone was recognizable until the end of the treatment. On the contrary, in spheres treated with Se-3-AP at 10 μM, the proliferative rim could be seen on the day 6 to finally disappear on the day 8, whereas quiescent zone was visually merged with necrotic core from the day 6. These facts indicate the possibility that living cells in spheres incubated with 10 μM of Se-3-AP derive from quiescent zone and are more affected by hypoxia. Therefore, it is possible that challenged hypoxic conditions in 3-D cultures subjected to Se-3-AP at 10 μM affects Oct-4 expression in correlation with non-significant changes in MFI values of these spheroids compared to non-treated controls, despite noteworthy decrease in percentage of Oct-4-expresing cells. On the other hand, 100 μM Se-3-AP brought all the benefits, including superior control of 3-D tumor growth, threefold decrease in percentage of Oct-4-expresing cells, as well as statistically significant restriction in number of mRNA copies within the remaining Oct-4 transcribing cells. It is obvious that cells that survived treatment with Se-3-AP at 100 μM did not raise expression of this gene as it was reported in other cases (Magnifico et al., 2009; Saigusa et al., 2009; Zhang et al., 2010). Thus, this result is the solid proof that Se-3-AP has the ability to induce phenotype reprogramming of 3-D breast cancer tumors.

Cellular generation of ·OH, which typically occurs by metal mediated H_2O_2 reduction, is the major cause of DNA damage in human cells (Bar-Or et al., 2001; Battin et al., 2011). This is linked to development of cancer (Zimmerman et al., 2015). Here we used the assay for determination of inhibition of Cu (I)-mediated oxidative DNA damage to compare activities of Se-3-AP and 3-AP (Battin et al., 2011). Complete neutralization of free reactive species and protection of plasmid SC form has been accomplished with 3-AP in concentration of 50 μM, whereas starting from the next concentration level (100 μM) nuclease activity became evident which emerged as a result of 3-AP complexation with Cu from the reactive mixture. The addition of Se-3-AP also resulted in concentration-dependently decrease in quantity of generated NC form, but its disappearance was attained when Se-3-AP was added to reaction mixture in concentration of 100 μM which coincided with creation of Cu complex and pUC19 DNA degradation. Our results showed that in DPPH test, Se-3-AP appear to be more potent antioxidant than 3-AP. It was not possible to establish correlation between free radical-scavenging activity and protection abilities of compounds, since 3-AP protected DNA at lower concentrations in comparison to Se-3-AP.

The side effects of anticancer agents are the most common causes that may limit their clinical use. During the pre-clinical and clinical studies, it was found that 3-AP increases the oxidation of Hb to metHb, which cannot transport oxygen causing methemoglobinemia, hypoxia and cyanosis (Kunos et al., 2010; Kunos et al., 2012; Ma et al., 2008; Stefani et al., 2013). This side effect of 3-AP significantly limits its clinical use, especially in patients with impaired cardiopulmonary function. In the design of new anticancer agents, which will be more efficient than 3-AP, it is very important to avoid this side effect of 3-AP. According to the results of the in vitro experiment, one can conclude that 3-AP was significantly more effective than Se-3-AP in oxidation of Hb to metHb. Several studies have been reported that the redox-active complexes of chelators and iron or copper ions, especially those with iron ions, are more effective than chelators themselves in increasing metHb generation (Basha et al., 2016; Quach et al., 2012). Despite the structural similarity of Se-3-AP and 3-AP, the differences between the redox-active complexes of Se-3-AP and 3-AP, as well as different redox potentials could cause the difference in ability of the Se-3-AP and 3-AP to catalyze metHb formation. Because Se-3-AP shows a lower ability for metHb formation compared to 3-AP, it can be assumed that Se-3-AP has more favorable toxicological profile than 3-AP, especially knowing that individuals with metHb content lower than 10% in blood serum do not show any clinical symptoms (Adams et al., 2007).

HSA is the most abundant protein of blood plasma can bind a remarkable variety of drugs impacting their delivery and efficacy. HSA not only protects the bound drugs against oxidation, but also alters the pharmacokinetic and pharmacodynamics properties of drugs and influences the in vivo drug distribution (Yang et al., 2014). In order to evaluate possibility for Se-3-AP delivery with HSA through blood we investigated Se-3-AP interaction with HSA. The results showed that Se-3-AP quenches HSA intrinsic fluorescence in a concentration-dependent manner, suggesting HSA–Se-3-AP adducts formation. The obtained values for K_{sv} and k_q point out to the static type mechanism of fluorophore quenching. The obtained negative value for ΔH and positive value for ΔS indicate that the electrostatic forces are the main contributors to HSA–Se-3-AP binding according to Ross' view (Ross and Subramanian, 1981). The calculated k_q values suggest that the binding between Se-3-AP and HSA is moderate, which is also predicted by the docking study. Results indicate that Se-3-AP can be effectively transported and stored by HSA. As the values of n at three different temperatures are very close to 1, Se-3-AP binds only to one binding site of HSA.

Results of the *Artemia salina* lethality assay provide additional testimony to Se-3-AP favorable toxicity profile. This assay is widely utilized model for evaluation of toxicity for compounds of diverse structures and modes of activity, such as anesthetics (Robinson et al., 1965), morphine-like compounds (Richter and Goldstein, 1970), cocarcinogenicity of phorbol esters (Kinghorn et al., 1977), pesticide residues (Grosch, 1967), and new compounds with potentially therapeutic properties (Krstic et al., 2014; Vanhaecke et al., 1981). Although results of *Artemia salina* lethality in context of compounds with anticancer properties were usually discussed as complementary indicator of the drug's activity (Krstic et al., 2014), those actually signify on its toxicity against non-malignant cells. This experimental model has no established cut-off LC_{50} value or grade scale that might be used for interpretation of toxicity level for any investigated compound. Previously, Meyer et al. (1982) postulated that compounds with $LC_{50} \leq 1.0$ mg/mL are known to possess toxic effects. However, due to variable sensitivity of *Artemia* species (Ruebhart et al., 2008), treatment with $K_2Cr_2O_7$ is usually used as an internal control for evaluation of toxicity. Comparing current LC_{50} for $K_2Cr_2O_7$ and the one published by Meyer et al. (1982) makes obvious that brine shrimps in our laboratory revealed about fourfold higher sensitivity. This fact discards the use of proposed LC_{50} concentration of 1 mg/mL for correlation of Se-3-AP with other compounds. Nevertheless, far

more important is the difference between toxicities of 3-AP and Se-3-AP. While Se-3-AP induced significantly higher percentage of apoptotic cells on both THP-1 and MCF-7 cell lines than 3-AP, its toxic activity on *Artemia salina* is twice lower. These results clearly indicate that Se-3-AP most probably possesses certain level of selectivity toward malignant compared to normal cells, which deserves detailed investigation in further studies.

5. Conclusion

Summarizing, we synthesized and characterized a selenium analog of 3-AP and investigated and compared biological modes of action of two isosteres. Se-3-AP revealed as more powerful apoptosis inducer than 3-AP, while both Se-3-AP and 3-AP induced concentration-dependent changes in cell cycle distribution. Apoptosis induced by Se-3-AP demonstrated high level of caspases dependency with upstream activation of intrinsic pathway. Se-3-AP stimulated phenotype-specific generation of mitochondrial $O_2^{\cdot}$ and dissipation of MTP in MCF-7 cells. Apart from its pro-apoptotic potential, Se-3-AP also revealed ability to challenge phenotype reprogramming of 3-D breast cancer tumors. It caused concentration-dependent changes in morphological features and growth rate of treated spheroids, as well as down regulation of Oct-4 gene expression. Se-3-AP showed lower ability for metHb formation compared to 3-AP, while acute lethality assay revealed its favorable toxicity profile. The presented data merit Se-3-AP as a putative candidate for further clinical development.

Acknowledgments

This Article is based upon work from COST Actions CA15135 and CA16119 supported by COST. The work was founded by grants PRIN 2015 no. 2015FCHJ8E (to R.S.) and by the Ministry of Education, Science and Technological Development of the Republic of Serbia (grant number 172055).

Appendix A. Supplementary material

Supplementary data associated with this article can be found, in the online version, at https://doi.org/10.1016/j.arabjc.2017.11.017.

References

Adams, V., Marley, J., McCarroll, C., 2007. Prilocaine induced methaemoglobinaemia in a medically compromised patient. Was this an inevitable consequence of the dose administered? Br. Dent. J. 203, 585–587.

Aggarwal, B.B., Sethi, G., Baladandayuthapani, V., Krishnan, S., Shishodia, S., 2007. Targeting cell signaling pathways for drug discovery: An old lock needs a new key. J. Cell. Biochem. 102, 580–592.

Agrawal, K.C., Booth, B.A., Michaud, R.L., Moore, E.C., Sartorelli, A.C., 1974. Comparative studies of the antineoplastic activity of 5-hydroxy-2-formylpyridine thiosemicarbazone and its seleno- semicarbazone, guanylhydrazone and semicarbazone analogs. Biochem. Pharmacol. 23, 2421–2429.

Al-Eisawi, Z., Stefani, C., Jansson, P.J., Arvind, A., Sharpe, P.C., Basha, M.T., Iskander, G.M., Kumar, N., Kovacevic, Z., Lane, D. J., Sahni, S., Bernhardt, P.V., Richardson, D.R., Kalinowski, D.S., 2016. Novel Mechanism of Cytotoxicity for the Selective Selenosemicarbazone, 2-Acetylpyridine 4,4-Dimethyl-3-selenosemicarbazone (Ap44mSe): Lysosomal Membrane Permeabilization. J. Med. Chem. 59, 294–312.

Albert, A., Serjeant, E.P., 1984. The Determination of Ionization Constants. Springer, Netherlands, Dordrecht.

Alvero, A.B., Chen, W., Sartorelli, A.C., Schwartz, P., Rutherford, T., Mor, G., 2006. Triapine (3-aminopyridine-2-carboxaldehyde thiosemicarbazone) induces apoptosis in ovarian cancer cells. J. Soc. Gynecol. Investig. 13, 145–152.

Andrzejewski, S., Gravel, S.P., Pollak, M., St-Pierre, J., 2014. Metformin directly acts on mitochondria to alter cellular bioenergetics. Cancer Metab. 2, 12.

Avery, T.L., Finch, R.A., Vasquez, K.M., Radparvar, S., Hanna, N. B., Revankar, G.R., Robins, R.K., 1990. Chemotherapeutic characterization in mice of 2-amino-9-beta-D-ribofuranosylpurine-6-sulfinamide (sulfinosine), a novel purine nucleoside with unique antitumor properties. Cancer Res. 50, 2625–2630.

Aye, Y., Long, M.J., Stubbe, J., 2012. Mechanistic studies of semicarbazone triapine targeting human ribonucleotide reductase in vitro and in mammalian cells: tyrosyl radical quenching not involving reactive oxygen species. J. Biol. Chem. 287, 35768–35778.

Bar-Or, D., Thomas, G.W., Rael, L.T., Lau, E.P., Winkler, J.V., 2001. Asp-Ala-His-Lys (DAHK) inhibits copper-induced oxidative DNA double strand breaks and telomere shortening. Biochem. Biophys. Res. Commun. 282, 356–360.

Barker, C.A., Burgan, W.E., Carter, D.J., Cerna, D., Gius, D., Hollingshead, M.G., Camphausen, K., Tofilon, P.J., 2006. In vitro and in vivo radiosensitization induced by the ribonucleotide reductase inhibitor Triapine (3-aminopyridine-2-carboxaldehyde-thiosemicarbazone). Clin. Cancer Res. 12, 2912–2918.

Basha, M.T., Bordini, J., Richardson, D.R., Martinez, M., Bernhardt, P.V., 2016. Kinetico-mechanistic studies on methemoglobin generation by biologically active thiosemicarbazone iron(III) complexes. J. Inorg. Biochem. 162, 326–333.

Battin, E.E., Zimmerman, M.T., Ramoutar, R.R., Quarles, C.E., Brumaghim, J.L., 2011. Preventing metal-mediated oxidative DNA damage with selenium compounds. Metallomics 3, 503–512.

Bertrand, P., Saintigny, Y., Lopez, B.S., 2004. p53's double life: transactivation-independent repression of homologous recombination. Trends Genet. 20, 235–243.

Calcatierra, V., Lopez, O., Fernandez-Bolanos, J.G., Plata, G.B., Padron, J.M., 2015. Phenolic thio- and selenosemicarbazones as multi-target drugs. Eur. J. Med. Chem. 94, 63–72.

Castle, T.C., Maurer, R.I., Sowrey, F.E., Went, M.J., Reynolds, C. A., McInnes, E.J., Blower, P.J., 2003. Hypoxia-targeting copper bis (selenosemicarbazone) complexes: comparison with their sulfur analogues. J. Am. Chem. Soc. 125, 10040–10049.

Combs Jr., G.F., 2015. Biomarkers of selenium status. Nutrients 7, 2209–2236.

Comsa, S., Cimpean, A.M., Raica, M., 2015. The story of MCF-7 breast cancer cell line: 40 years of experience in research. Anticancer Res. 35, 3147–3154.

Cory, J.G., Cory, A.H., Rappa, G., Lorico, A., Liu, M.C., Lin, T.S., Sartorelli, A.C., 1994. Inhibitors of ribonucleotide reductase. Comparative effects of amino- and hydroxy-substituted pyridine-2-carboxaldehyde thiosemicarbazones. Biochem. Pharmacol. 48, 335–344.

Cory, J.G., Cory, A.H., Rappa, G., Lorico, A., Liu, M.C., Lin, T.S., Sartorelli, A.C., 1995. Structure-function relationships for a new series of pyridine-2-carboxaldehyde thiosemicarbazones on ribonucleotide reductase activity and tumor cell growth in culture and in vivo. Adv. Enzyme Regul. 35, 55–68.

Covello, K.L., Kehler, J., Yu, H., Gordan, J.D., Arsham, A.M., Hu, C.J., Labosky, P.A., Simon, M.C., Keith, B., 2006. HIF-2alpha regulates Oct-4: effects of hypoxia on stem cell function, embryonic development, and tumor growth. Genes Dev. 20, 557–570.

Curry, S., Mandelkow, H., Brick, P., Franks, N., 1998. Crystal structure of human serum albumin complexed with fatty acid reveals an asymmetric distribution of binding sites. Nat. Struct. Biol. 5, 827–835.

Dai, X., Ge, J., Wang, X., Qian, X., Zhang, C., Li, X., 2013. OCT4 regulates epithelial-mesenchymal transition and its knockdown inhibits colorectal cancer cell migration and invasion. Oncol. Rep. 29, 155–160.

DeConti, R.C., Toftness, B.R., Agrawal, K.C., Tomchick, R., Mead, J.A., Bertino, J.R., Sartorelli, A.C., Creasey, W.A., 1972. Clinical and pharmacological studies with 5-hydroxy-2-formylpyridine thiosemicarbazone. Cancer Res. 32, 1455–1462.

Dunning, J., Hay, P.J., 1977. Methods of Electronic Structure Theory. Springer, US, Boston, MA.

Emhemmed, F., Ali, A.S., Zhao, Q., Appert-Collin, A., Bennasroune, A., Schini-Kerth, V.B., Muller, C.D., Desaubry, L., Fuhrmann, G., 2017. Pro-differentiating effects of a synthetic flavagline on human teratocarcinomal cancer stem-like cells. Cell Biol. Toxicol. 33, 295–306.

Enyedy, E.A., Nagy, N.V., Zsigo, E., Kowol, C.R., Arion, V.B., Keppler, B.K., Kiss, T., 2010. Comparative Solution Equilibrium Study of the Interactions of Copper(II), Iron(II) and Zinc(II) with Triapine (3-Aminopyridine-2-carbaldehyde Thiosemicarbazone) and Related Ligands. Eur. J. Inorg. Chem. 2010, 1717–1728.

Enyedy, E.A., Primik, M.F., Kowol, C.R., Arion, V.B., Kiss, T., Keppler, B.K., 2011. Interaction of Triapine and related thiosemicarbazones with iron(III)/(II) and gallium(III): a comparative solution equilibrium study. Dalton Trans. 40, 5895–5905.

Filipovic, N., Polovic, N., Raskovic, B., Misirlic-Dencic, S., Dulovic, M., Savic, M., Niksic, M., Mitic, D., Andjelkovic, K., Todorovic, T., 2014. Biological activity of two isomeric N-heteroaromatic selenosemicarbazones and their metal complexes. Monatsh. Chem. 145, 1089–1099.

Filipovic, N.R., Bjelogrlic, S., Marinkovic, A., Verbic, T.Z., Cvijetic, I.N., Sencanski, M., Rodic, M., Vujcic, M., Sladic, D., Strikovic, Z., Todorovic, T.R., Muller, C.D., 2015. Zn(ii) complex with 2-quinolinecarboxaldehyde selenosemicarbazone: synthesis, structure, interaction studies with DNA/HSA, molecular docking and caspase-8 and -9 independent apoptose induction. RSC Adv. 5, 95191–95211.

Filipovic, N.R., Bjelogrlic, S., Portalone, G., Pelliccia, S., Silvestri, R., Klisuric, O., Sencanski, M., Stankovic, D., Todorovic, T.R., Muller, C.D., 2016. Pro-apoptotic and pro-differentiation induction by 8-quinolinecarboxaldehyde selenosemicarbazone and its Co (iii) complex in human cancer cell lines. Med. Chem. Commun. 7, 1604–1616.

Filipovic, N.R., Elshaflu, H., Grubisc, S., Jovanovic, L.S., Rodic, M., Novakovic, I., Malesevic, A., Djordjevic, I.S., Li, H., Sojic, N., Marinkovic, A., Todorovic, T.R., 2017. Co(III) complexes of (1,3-selenazol-2-yl)hydrazones and their sulphur analogues. Dalton Trans. 46, 2910–2924.

Finch, R.A., Liu, M.C., Cory, A.H., Cory, J.G., Sartorelli, A.C., 1999. Triapine (3-aminopyridine-2-carboxaldehyde thiosemicarbazone; 3-AP): an inhibitor of ribonucleotide reductase with antineoplastic activity. Adv Enzyme Regul. 39, 3–12.

Finch, R.A., Liu, M., Grill, S.P., Rose, W.C., Loomis, R., Vasquez, K.M., Cheng, Y., Sartorelli, A.C., 2000. Triapine (3-aminopyridine-2-carboxaldehyde- thiosemicarbazone): a potent inhibitor of ribonucleotide reductase activity with broad spectrum antitumor activity. Biochem. Pharmacol. 59, 983–991.

Finley, L.W., Carracedo, A., Lee, J., Souza, A., Egia, A., Zhang, J., Teruya-Feldstein, J., Moreira, P.I., Cardoso, S.M., Clish, C.B., Pandolfi, P.P., Haigis, M.C., 2011. SIRT3 opposes reprogramming of cancer cell metabolism through HIF1alpha destabilization. Cancer Cell 19, 416–428.

Fontanesi, F., 2015. Mitochondria: Structure and Role in Respiration. In: eLS. John Wiley & Sons, Ltd, Chichester, UK, pp. 1–13. https://doi.org/10.1002/9780470015902.a0001380.pub2.

French, F.A., Blanz Jr., E.J., Shaddix, S.C., Brockman, R.W., 1974. Alpha-(N)-formylheteroaromatic thiosemicarbazones. Inhibition of tumor-derived ribonucleoside diphosphate reductase and correlation with in vivo antitumor activity. J. Med. Chem. 17, 172–181.

Frisch, M.J., Trucks, G.W., Schlegel, H.B., Scuseria, G.E., Robb, M. A., Cheeseman, J.R.S., Barone, V., Mennucci, B., Petersson, G.A., Nakatsuji, H., Caricato, M., Li, X., Hratchian, H.P., Izmaylov, A. F., Bloino, J., Zheng, G., Sonnenberg, J.L., Hada, M., Ehara, M., Toyota, K., Fukuda, R., Hasegawa, J., Ishida, M., Nakajima, T., Honda, Y., Kitao, O., Nakai, H., Vreven, T., Montgomery Jr., J. A., Peralta, J.E., Ogliaro, F., Bearpark, M., Heyd, J.J., Brothers, E., Kudin, K.N., Staroverov, V.N., Kobayashi, R., Normand, J., Raghavachari, K., Rendell, A., Burant, J.C., Iyengar, S.S., Tomasi, J., Cossi, M., Rega, N., Millam, J.M., Klene, M., Knox, J.E., Cross, J.B., Bakken, V., Adamo, C., Jaramillo, J., Gomperts, R., Stratmann, R.E., Yazyev, O., Austin, A.J., Cammi, R., Pomelli, C., Ochterski, J.W., Martin, R.L., Morokuma, K., Zakrzewski, V.G., Voth, G.A., Salvador, P., Dannenberg, J.J., Dapprich, S., Daniels, A.D., Farkas, O., Foresman, J.B., Ortiz, J.V., Cioslowski, J., Fox, D.J., 2016. Gaussian 09, Revision D.01. Gaussian Inc., Wallingford, CT.

Fukai, T., Ushio-Fukai, M., 2011. Superoxide dismutases: role in redox signaling, vascular function, and diseases. Antioxid. Redox Signal. 15, 1583–1606.

Galluzzi, L., Joza, N., Tasdemir, E., Maiuri, M.C., Hengartner, M., Abrams, J.M., Tavernarakis, N., Penninger, J., Madeo, F., Kroemer, G., 2008. No death without life: vital functions of apoptotic effectors. Cell Death Differ. 15, 1113–1123.

Galluzzi, L., Morselli, E., Kepp, O., Vitale, I., Rigoni, A., Vacchelli, E., Michaud, M., Zischka, H., Castedo, M., Kroemer, G., 2010. Mitochondrial gateways to cancer. Mol. Aspects Med. 31, 1–20.

Gatz, S.A., Wiesmuller, L., 2006. p53 in recombination and repair. Cell Death Differ. 13, 1003–1016.

Ghuman, J., Zunszain, P.A., Petitpas, I., Bhattacharya, A.A., Otagiri, M., Curry, S., 2005. Structural basis of the drug-binding specificity of human serum albumin. J. Mol. Biol. 353, 38–52.

Grimes, D.R., Kelly, C., Bloch, K., Partridge, M., 2014. A method for estimating the oxygen consumption rate in multicellular tumour spheroids. J. Roy. Soc. Interface 11, 20131124.

Grimme, S., 2006. Semiempirical GGA-type density functional constructed with a long-range dispersion correction. J. Comput. Chem. 27, 1787–1799.

Grosch, D.S., 1967. Poisoning with DDT: effect on reproductive performance of Artemia. Science 155, 592–593.

Gupta, P.B., Fillmore, C.M., Jiang, G., Shapira, S.D., Tao, K., Kuperwasser, C., Lander, E.S., 2011. Stochastic state transitions give rise to phenotypic equilibrium in populations of cancer cells. Cell 146, 633–644.

Hay, P.J., Wadt, W.R., 1985. Ab initio effective core potentials for molecular calculations. Potentials for the transition metal atoms Sc to Hg. J. Chem. Phys. 82, 270–283.

He, X.M., Carter, D.C., 1992. Atomic structure and chemistry of human serum albumin. Nature 358, 209–215.

Heffeter, P., Pirker, C., Kowol, C.R., Herrman, G., Dornetshuber, R., Miklos, W., Jungwirth, U., Koellensperger, G., Keppler, B.K., Berger, W., 2012. Impact of terminal dimethylation on the resistance profile of alpha-N-heterocyclic thiosemicarbazones. Biochem. Pharmacol. 83, 1623–1633.

Hogemann-Savellano, D., Bos, E., Blondet, C., Sato, F., Abe, T., Josephson, L., Weissleder, R., Gaudet, J., Sgroi, D., Peters, P. J., Basilion, J.P., 2003. The transferrin receptor: a potential molecular imaging marker for human cancer. Neoplasia 5, 495–506.

Hu, J., Qin, K., Zhang, Y., Gong, J., Li, N., Lv, D., Xiang, R., Tan, X., 2011. Downregulation of transcription factor Oct4 induces an epithelial-to-mesenchymal transition via enhancement of Ca^{2+} influx in breast cancer cells. Biochem. Biophys. Res. Commun. 411, 786–791.

Ishiguro, K., Lin, Z.P., Penketh, P.G., Shyam, K., Zhu, R., Baumann, R.P., Zhu, Y.L., Sartorelli, A.C., Rutherford, T.J., Ratner, E.S., 2014. Distinct mechanisms of cell-kill by triapine and its terminally dimethylated derivative Dp44mT due to a loss or gain of activity of their copper(II) complexes. Biochem. Pharmacol. 91, 312–322.

Jimbo, A., Fujita, E., Kouroku, Y., Ohnishi, J., Inohara, N., Kuida, K., Sakamaki, K., Yonehara, S., Momoi, T., 2003. ER stress induces caspase-8 activation, stimulating cytochrome c release and caspase-9 activation. Exp. Cell Res. 283, 156–166.

Jordheim, L.P., Guittet, O., Lepoivre, M., Galmarini, C.M., Dumontet, C., 2005. Increased expression of the large subunit of ribonucleotide reductase is involved in resistance to gemcitabine in human mammary adenocarcinoma cells. Mol. Cancer Ther. 4, 1268–1276.

Kalinowski, D.S., Richardson, D.R., 2005. The evolution of iron chelators for the treatment of iron overload disease and cancer. Pharmacol. Rev. 57, 547–583.

Karoubi, G., Gugger, M., Schmid, R., Dutly, A., 2009. OCT4 expression in human non-small cell lung cancer: implications for therapeutic intervention. Interact. Cardiovasc. Thorac. Surg. 8, 393–397.

Karp, J.E., Giles, F.J., Gojo, I., Morris, L., Greer, J., Johnson, B., Thein, M., Sznol, M., Low, J., 2008. A phase I study of the novel ribonucleotide reductase inhibitor 3-aminopyridine-2-carboxaldehyde thiosemicarbazone (3-AP, Triapine) in combination with the nucleoside analog fludarabine for patients with refractory acute leukemias and aggressive myeloproliferative disorders. Leuk. Res. 32, 71–77.

Katoh, I., Tomimori, Y., Ikawa, Y., Kurata, S., 2004. Dimerization and processing of procaspase-9 by redox stress in mitochondria. J. Biol. Chem. 279, 15515–15523.

Kim, R.J., Nam, J.S., 2011. OCT4 Expression enhances features of cancer stem cells in a mouse model of breast cancer. Lab. Anim. Res. 27, 147–152.

Kinghorn, A.D., Harjes, K.K., Doorenbos, N.J., 1977. Screening procedure for phorbol esters using brine shrimp (Artemia salina) larvae. J. Pharm. Sci. 66, 1362–1363.

Klayman, D.L., Scovill, J.P., Mason, C.J., Bartosevich, J.F., Bruce, J., Lin, A.J., 1983. 2-Acetylpyridine thiosemicarbazones. 6.2-Acetylpyridine and 2-butyrylpyridine thiosemicarbazones as antileukemic agents. Arzneimittelforschung 33, 909–912.

Knox, J.J., Hotte, S.J., Kollmannsberger, C., Winquist, E., Fisher, B., Eisenhauer, E.A., 2007. Phase II study of Triapine in patients with metastatic renal cell carcinoma: a trial of the National Cancer Institute of Canada Clinical Trials Group (NCIC IND.161). Invest. New Drugs 25, 471–477.

Kong, D., Banerjee, S., Ahmad, A., Li, Y., Wang, Z., Sethi, S., Sarkar, F.H., 2010. Epithelial to mesenchymal transition is mechanistically linked with stem cell signatures in prostate cancer cells. PLoS One 5, e12445.

Kowol, C.R., Reisner, E., Chiorescu, I., Arion, V.B., Galanski, M., Deubel, D.V., Keppler, B.K., 2008. An electrochemical study of antineoplastic gallium, iron and ruthenium complexes with redox noninnocent alpha-N-heterocyclic chalcogensemicarbazones. Inorg. Chem. 47, 11032–11047.

Kowol, C.R., Trondl, R., Heffeter, P., Arion, V.B., Jakupec, M.A., Roller, A., Galanski, M., Berger, W., Keppler, B.K., 2009. Impact of metal coordination on cytotoxicity of 3-aminopyridine-2-carboxaldehyde thiosemicarbazone (triapine) and novel insights into terminal dimethylation. J. Med. Chem. 52, 5032–5043.

Kowol, C.R., Trondl, R., Arion, V.B., Jakupec, M.A., Lichtscheidl, I., Keppler, B.K., 2010. Fluorescence properties and cellular distribution of the investigational anticancer drug triapine (3-aminopyridine-2-carboxaldehyde thiosemicarbazone) and its zinc (II) complex. Dalton Trans. 39, 704–706.

Kowol, C.R., Heffeter, P., Miklos, W., Gille, L., Trondl, R., Cappellacci, L., Berger, W., Keppler, B.K., 2012. Mechanisms underlying reductant-induced reactive oxygen species formation by anticancer copper(II) compounds. J. Biol. Inorg. Chem. 17, 409–423.

Kowol, C.R., Miklos, W., Pfaff, S., Hager, S., Kallus, S., Pelivan, K., Kubanik, M., Enyedy, E.A., Berger, W., Heffeter, P., Keppler, B. K., 2016. Impact of stepwise NH2-methylation of triapine on the physicochemical properties, anticancer activity, and resistance circumvention. J. Med. Chem. 59, 6739–6752.

Krishnan, R., Binkley, J.S., Seeger, R., Pople, J.A., 1980. Self-consistent molecular orbital methods. XX. A basis set for correlated wave functions. J. Chem. Phys. 72, 650–654.

Kroemer, G., Galluzzi, L., Brenner, C., 2007. Mitochondrial membrane permeabilization in cell death. Physiol. Rev. 87, 99–163.

Krstic, N.M., Matic, I.Z., Juranic, Z.D., Novakovic, I.T., Sladic, D. M., 2014. Steroid dimers-in vitro cytotoxic and antimicrobial activities. J. Steroid Biochem. Mol. Biol. 143, 365–375.

Kunos, C.A., Waggoner, S., Von Gruenigen, V., Eldermire, E., Pink, J., Dowlati, A., Kinsella, T.J., 2010. Phase I trial of pelvic radiation, weekly cisplatin, and 3-aminopyridine-2-carboxaldehyde thiosemicarbazone (3-AP, NSC #663249) for locally advanced cervical cancer. Clin. Cancer Res. 16, 1298–1306.

Kunos, C.A., Radivoyevitch, T., Ingalls, S.T., Hoppel, C.L., 2012. Management of 3-aminopyridine-2-carboxaldehyde thiosemicarbazone-induced methemoglobinemia. Future Oncol. 8, 145–150.

Lahm, H., Doppler, S., Dressen, M., Werner, A., Adamczyk, K., Schrambke, D., Brade, T., Laugwitz, K.L., Deutsch, M.A., Schiemann, M., Lange, R., Moretti, A., Krane, M., 2015. Live fluorescent RNA-based detection of pluripotency gene expression in embryonic and induced pluripotent stem cells of different species. Stem Cells 33, 392–402.

Lakovicz, J.R., 2006. Principles of Fluorescence Spectroscopy. Springer, US, Boston, MA.

Leitch, C., Osdal, T., Andresen, V., Molland, M., Kristiansen, S., Nguyen, X.N., Bruserud, O., Gjertsen, B.T., McCormack, E., 2016. Hydroxyurea synergizes with valproic acid in wild-type p53 acute myeloid leukaemia. Oncotarget 7, 8105–8118.

Li, Q., Yang, W.y., Qu, L.l., Qi, H.Y., Huang, Y., Zhang, Z., 2014. Interaction of warfarin with human serum albumin and effect of ferulic acid on the binding. J. Spectrosc., 1–7

Li, X., Yang, Z., 2015. Interaction of oridonin with human serum albumin by isothermal titration calorimetry and spectroscopic techniques. Chem. Biol. Interact. 232, 77–84.

Lin, R.Z., Chang, H.Y., 2008. Recent advances in three-dimensional multicellular spheroid culture for biomedical research. Biotechnol. J. 3, 1172–1184.

Lin, Z.P., Ratner, E.S., Whicker, M.E., Lee, Y., Sartorelli, A.C., 2014. Triapine disrupts CtIP-mediated homologous recombination repair and sensitizes ovarian cancer cells to PARP and topoisomerase inhibitors. Mol. Cancer Res. 12, 381–393.

Liu, D.P., Song, H., Xu, Y., 2010. A common gain of function of p53 cancer mutants in inducing genetic instability. Oncogene 29, 949–956.

Liu, M.C., Lin, T.S., Cory, J.G., Cory, A.H., Sartorelli, A.C., 1996. Synthesis and biological activity of 3- and 5-amino derivatives of pyridine-2-carboxaldehyde thiosemicarbazone. J. Med. Chem. 39, 2586–2593.

Liu, M.C., Lin, T.S., Sartorelli, A.C., 1992. Synthesis and antitumor activity of amino derivatives of pyridine-2-carboxaldehyde thiosemicarbazone. J. Med. Chem. 35, 3672–3677.

Ma, B., Goh, B.C., Tan, E.H., Lam, K.C., Soo, R., Leong, S.S., Wang, L.Z., Mo, F., Chan, A.T., Zee, B., Mok, T., 2008. A multicenter phase II trial of 3-aminopyridine-2-carboxaldehyde thiosemicarbazone (3-AP, Triapine) and gemcitabine in advanced non-small-cell lung cancer with pharmacokinetic evaluation using peripheral blood mononuclear cells. Invest. New Drugs 26, 169–173.

Magnifico, A., Albano, L., Campaner, S., Delia, D., Castiglioni, F., Gasparini, P., Sozzi, G., Fontanella, E., Menard, S., Tagliabue, E.,

2009. Tumor-initiating cells of HER2-positive carcinoma cell lines express the highest oncoprotein levels and are sensitive to trastuzumab. Clin. Cancer Res. 15, 2010–2021.
Mautner, H.G., Kumler, W.D., Okano, Y., Pratt, R., 1956. Antifungal activity of some substituted selenosemicarbazones and related compounds. Antibiot. Chemother. 6, 51–55.
McLean, A.D., Chandler, G.S., 1980. Contracted Gaussian basis sets for molecular calculations. I. Second row atoms, Z = 11-18. J. Chem. Phys. 72, 5639–5648.
Mekeel, K.L., Tang, W., Kachnic, L.A., Luo, C.M., DeFrank, J.S., Powell, S.N., 1997. Inactivation of p53 results in high rates of homologous recombination. Oncogene 14, 1847–1857.
Meyer, B.N., Ferrigni, N.R., Putnam, J.E., Jacobsen, L.B., Nichols, D.E., McLaughlin, J.L., 1982. Brine shrimp: a convenient general bioassay for active plant constituents. Planta Med. 45, 31–34.
Mitchell, P., Moyle, J., 1965a. Evidence discriminating between the chemical and the chemiosmotic mechanisms of electron transport phosphorylation. Nature 208, 1205–1206.
Mitchell, P., Moyle, J., 1965b. Stoichiometry of proton translocation through the respiratory chain and adenosine triphosphatase systems of rat liver mitochondria. Nature 208, 147–151.
Mohan, C.D., Srinisava, V., Rangappa, S., Mervin, L., Mohan, S., Paricharak, S., Baday, S., Li, F., Shanmugam, M.K., Chinnathambi, A., Zayed, M.E., Alharbi, S.A., Bender, A., Sethi, G., Bassapa, S., Rangappa, K.S., 2016. Trisubstituated-imidazoles induce apoptosis in human breast cancer cells by targeting the oncogenic PI3K/Akt/mTOR signaling pathway. PLoS One 11, e0153155.
Molter, A., Rust, J., Lehmann, C.W., Deepa, G., Chiba, P., Mohr, F., 2011. Synthesis, structures and anti-malaria activity of some gold(I) phosphine complexes containing seleno- and thiosemicarbazonato ligands. Dalton Trans. 40, 9810–9820.
Moorthy, N.S., Cerqueira, N.M., Ramos, M.J., Fernandes, P.A., 2013. Development of ribonucleotide reductase inhibitors: a review on structure activity relationships. Mini. Rev. Med. Chem. 13, 1862–1872.
Morris, G.M., Huey, R., Lindstrom, W., Sanner, M.F., Belew, R.K., Goodsell, D.S., Olson, A.J., 2009. AutoDock4 and AutoDockTools4: Automated docking with selective receptor flexibility. J. Comput. Chem. 30, 2785–2791.
Mortazavi, A., Ling, Y., Martin, L.K., Wei, L., Phelps, M.A., Liu, Z., Harper, E.J., Ivy, S.P., Wu, X., Zhou, B.S., Liu, X., Deam, D., Monk, J.P., Hicks, W.J., Yen, Y., Otterson, G.A., Grever, M.R., Bekaii-Saab, T., 2013. A phase I study of prolonged infusion of triapine in combination with fixed dose rate gemcitabine in patients with advanced solid tumors. Invest. New Drugs 31, 685–695.
Myers, C.R., 2016. Enhanced targeting of mitochondrial peroxide defense by the combined use of thiosemicarbazones and inhibitors of thioredoxin reductase. Free Radic. Biol. Med. 91, 81–92.
Myers, J.M., Antholine, W.E., Zielonka, J., Myers, C.R., 2011. The iron-chelating drug triapine causes pronounced mitochondrial thiol redox stress. Toxicol. Lett. 201, 130–136.
Myers, J.M., Cheng, Q., Antholine, W.E., Kalyanaraman, B., Filipovska, A., Arner, E.S., Myers, C.R., 2013. Redox activation of Fe(III)-thiosemicarbazones and Fe(III)-bleomycin by thioredoxin reductase: specificity of enzymatic redox centers and analysis of reactive species formation by ESR spin trapping. Free Radic. Biol. Med. 60, 183–194.
Niu, C., Li, J., Doyle, T.W., Chen, S.h., Pharmaceuticals, V., Park, S., Haven, N., 1998. Synthesis of 3-Aminopyridine-2-carboxaidehyde Thiosemicarbazone (3-AP). Tetrahedron 54, 6311–6318.
Nordlund, P., Reichard, P., 2006. Ribonucleotide reductases. Annu. Rev. Biochem. 75, 681–706.
Papa, L., Hahn, M., Marsh, E.L., Evans, B.S., Germain, D., 2014. SOD2 to SOD1 switch in breast cancer. J. Biol. Chem. 289, 5412–5416.
Pelivan, K., Miklos, W., van, S.S., Koellensperger, G., Gille, L., Berger, W., Heffeter, P., Kowol, C.R., Keppler, B.K., 2016. Differences in protein binding and excretion of Triapine and its Fe (III) complex. J. Inorg. Biochem. 160, 61–69.
Pessoa, M.M.B., Andrade, G.F.S., Paoli Monteiro, V.R., Temperini, M.L.A., 2001. 2-Formylpyridinethiosemicarbazone and methyl derivatives: spectroscopic studies. Polyhedron 20, 3133–3141.
Pizzo, C., Faral-Tello, P., Salinas, G., Flo, M., Robello, C., Wipf, P., Mahler, S.G., 2012. Selenosemicarbazones as potent cruzipain inhibitors and their antiparasitic properties against Trypanosoma cruzi. Med. Chem. Commun. 3, 362–368.
Prior, R.L., Wu, X., Schaich, K., 2005. Standardized methods for the determination of antioxidant capacity and phenolics in foods and dietary supplements. J. Agric. Food Chem. 53, 4290–4302.
Quach, P., Gutierrez, E., Basha, M.T., Kalinowski, D.S., Sharpe, P. C., Lovejoy, D.B., Bernhardt, P.V., Jansson, P.J., Richardson, D. R., 2012. Methemoglobin formation by triapine, di-2-pyridylketone-4,4-dimethyl-3-thiosemicarbazone (Dp44mT), and other anticancer thiosemicarbazones: identification of novel thiosemicarbazones and therapeutics that prevent this effect. Mol. Pharmacol. 82, 105–114.
Ratner, E.S., Zhu, Y.L., Penketh, P.G., Berenblum, J., Whicker, M. E., Huang, P.H., Lee, Y., Ishiguro, K., Zhu, R., Sartorelli, A.C., Lin, Z.P., 2016. Triapine potentiates platinum-based combination therapy by disruption of homologous recombination repair. Br. J. Cancer 114, 777–786.
Revenko, M.D., Prisacari, V.I., Dizdari, A.V., Stratulat, E.F., Corja, I.D., Proca, L.M., 2011. Synthesis, antibacterial, and antifungal activities of 8-quinolinealdehyde chalcogensemicarbazones and their copper(II) complexes. Pharm. Chem. J. 45, 351–354.
Richter, J.A., Goldstein, A., 1970. The effects of morphine-like compounds on the light responses of the brine shrimp Artemia salina. Psychopharmacologia 17, 327–337.
Robinson, A.B., Manly, K.F., Anthony, M.P., Catchpool, J.F., Pauling, L., 1965. Anesthesia of Artemia larvae: method for quantitative study. Science 149, 1255–1258.
Ross, P.D., Subramanian, S., 1981. Thermodynamics of protein association reactions: forces contributing to stability. Biochemistry 20, 3096–3102.
Ruebhart, D.R., Cock, I.E., Shaw, G.R., 2008. Brine shrimp bioassay: importance of correct taxonomic identification of Artemia (Anostraca) species. Environ. Toxicol. 23, 555–560.
Saigusa, S., Tanaka, K., Toiyama, Y., Yokoe, T., Okugawa, Y., Ioue, Y., Miki, C., Kusunoki, M., 2009. Correlation of CD133, OCT4, and SOX2 in rectal cancer and their association with distant recurrence after chemoradiotherapy. Ann. Surg. Oncol. 16, 3488–3498.
Sanner, M.F., 1999. Python: a programming language for software integration and development. J. Mol. Graph. Model. 17, 57–61.
Schelman, W.R., Morgan-Meadows, S., Marnocha, R., Lee, F., Eickhoff, J., Huang, W., Pomplun, M., Jiang, Z., Alberti, D., Kolesar, J.M., Ivy, P., Wilding, G., Traynor, A.M., 2009. A phase I study of Triapine in combination with doxorubicin in patients with advanced solid tumors. Cancer Chemother. Pharmacol. 63, 1147–1156.
Shao, J., Zhou, B., Zhu, L., Qiu, W., Yuan, Y.C., Xi, B., Yen, Y., 2004. In vitro characterization of enzymatic properties and inhibition of the p53R2 subunit of human ribonucleotide reductase. Cancer Res. 64, 1–6.
Shao, J., Zhou, B., Di Bilio, A.J., Zhu, L., Wang, T., Qi, C., Shih, J., Yen, Y., 2006. A Ferrous-Triapine complex mediates formation of reactive oxygen species that inactivate human ribonucleotide reductase. Mol. Cancer Ther. 5, 586–592.
Stahlberg, A., Rusnakova, V., Kubista, M., 2013. The added value of single-cell gene expression profiling. Brief. Funct. Genomics 12, 81–89.
Stahlberg, A., Kubista, M., 2014. The workflow of single-cell expression profiling using quantitative real-time PCR. Expert. Rev Mol. Diagn. 14, 323–331.

Stefani, C., Jansson, P.J., Gutierrez, E., Bernhardt, P.V., Richardson, D.R., Kalinowski, D.S., 2013. Alkyl substituted 2′-benzoylpyridine thiosemicarbazone chelators with potent and selective anti-neoplastic activity: novel ligands that limit methemoglobin formation. J. Med. Chem. 56, 357–370.

Syn, N., Wang, L., Sethi, G., Thiery, J.P., Goh, B.C., 2016. Exosome-mediated metastasis: from epithelial-mesenchymal transition to escape from immunosurveillance. Trends Pharmacol. Sci. 37, 606–617.

Tao, R., Coleman, M.C., Pennington, J.D., Ozden, O., Park, S.H., Jiang, H., Kim, H.S., Flynn, C.R., Hill, S., Hayes, M.W., Olivier, A.K., Spitz, D.R., Gius, D., 2010. Sirt3-mediated deacetylation of evolutionarily conserved lysine 122 regulates MnSOD activity in response to stress. Mol. Cell 40, 893–904.

Todorovic, T.R., Bacchi, A., Sladic, D.M., Todorovic, N.M., Bozic, T.T., Radanovic, D.D., Filipovic, N.R., Pelizzi, G., Andjelkovic, K.K., 2009. Synthesis, characterization and biological activity evaluation of Pt(II), Pd(II), Co(III) and Ni(II) complexes with N-heteroaromatic selenosemicarbazones. Inorganica Chim. Acta 362, 3813–3820.

Todorovic, T.R., Vukasinovic, J., Portalone, G., Suleiman, S., Gligorijevic, N., Bjelogrlic, S., Jovanovic, K., Radulovic, S., Andelkovic, K., Cassar, A., Filipovic, N.R., Schembri-Wismayer, P., 2017. (Chalcogen)semicarbazones and their cobalt complexes differentiate HL-60 myeloid leukaemia cells and are cytotoxic towards tumor cell lines. Med. Chem. Commun. 8, 103–111.

Trondl, R., Flocke, L.S., Kowol, C.R., Heffeter, P., Jungwirth, U., Mair, G.E., Steinborn, R., Enyedy, E.A., Jakupec, M.A., Berger, W., Keppler, B.K., 2014. Triapine and a more potent dimethyl derivative induce endoplasmic reticulum stress in cancer cells. Mol. Pharmacol. 85, 451–459.

Trott, O., Olson, A.J., 2010. AutoDock Vina: improving the speed and accuracy of docking with a new scoring function, efficient optimization and multithreading. J. Comput. Chem. 31, 455–461.

Turk, S.R., Shipman Jr., C., Drach, J.C., 1986. Structure-activity relationships among alpha-(N)-heterocyclic acyl thiosemicarbazones and related compounds as inhibitors of herpes simplex virus type 1-specified ribonucleoside diphosphate reductase. J. Gen. Virol. 67 (Pt 8), 1625–1632.

Vanhaecke, P., Persoone, G., Claus, C., Sorgeloos, P., 1981. Proposal for a short-term toxicity test with Artemia nauplii. Ecotoxicol. Environ. Saf 5, 382–387.

Wadler, S., Makower, D., Clairmont, C., Lambert, P., Fehn, K., Sznol, M., 2004. Phase I and pharmacokinetic study of the ribonucleotide reductase inhibitor, 3-aminopyridine-2-carboxaldehyde thiosemicarbazone, administered by 96-hour intravenous continuous infusion. J. Clin. Oncol. 22, 1553–1563.

Walker, R.A., Day, S.J., 1986. Transferrin receptor expression in non-malignant and malignant human breast tissue. J. Pathol. 148, 217–224.

Wang, X.Q., Ongkeko, W.M., Chen, L., Yang, Z.F., Lu, P., Chen, K. K., Lopez, J.P., Poon, R.T., Fan, S.T., 2010. Octamer 4 (Oct4) mediates chemotherapeutic drug resistance in liver cancer cells through a potential Oct4-AKT-ATP-binding cassette G2 pathway. Hepatology 52, 528–539.

Wang, Z.M., Ho, J.X., Ruble, J.R., Rose, J., Ruker, F., Ellenburg, M., Murphy, R., Click, J., Soistman, E., Wilkerson, L., Carter, D. C., 2013. Structural studies of several clinically important oncology drugs in complex with human serum albumin. Biochim. Biophys. Acta 1830, 5356–5374.

West, D.X., Ahrweiler, P.M., Ertem, G., Scovill, J.P., Klayman, D. L., Flippen-Anderson, J.L., Gilardi, R., George, C., Pannell, L.K., 1985. Iron(III) complexes of some thiosemicarbazones derived from 2-acetylpyridine, its 6-methyl derivative and itsN-oxide. Transit. Metal Chem. 10, 264–270.

Whitnall, M., Howard, J., Ponka, P., Richardson, D.R., 2006. A class of iron chelators with a wide spectrum of potent antitumor activity that overcomes resistance to chemotherapeutics. Proc. Natl. Acad. Sci. USA 103, 14901–14906.

Winterbourn, C.C., Carrell, R.W., 1977. Oxidation of human haemoglobin by copper. Mechanism and suggested role of the thiol group of residue beta-93. Biochem. J. 165, 141–148.

Yang, F., Zhang, Y., Liang, H., 2014. Interactive association of drugs binding to human serum albumin. Int. J. Mol. Sci. 15, 3580–3595.

Yu, Y., Wong, J., Lovejoy, D.B., Kalinowski, D.S., Richardson, D. R., 2006. Chelators at the cancer coalface: desferrioxamine to Triapine and beyond. Clin. Cancer Res. 12, 6876–6883.

Zhang, X., Han, B., Huang, J., Zheng, B., Geng, Q., Aziz, F., Dong, Q., 2010. Prognostic significance of OCT4 expression in adenocarcinoma of the lung. Jpn. J. Clin. Oncol. 40, 961–966.

Zimmerman, M.T., Bayse, C.A., Ramoutar, R.R., Brumaghim, J.L., 2015. Sulfur and selenium antioxidants: challenging radical scavenging mechanisms and developing structure-activity relationships based on metal binding. J. Inorg. Biochem. 145, 30–40.